Phytomedicine 145 (2025) 156994

Contents lists available at ScienceDirect

Phytomedicine

journal homepage: www.elsevier.com/locate/phymed

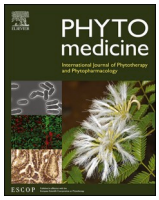

Original Article

Tanshinone I alleviates post-ischemic myocardial injury by targeting TGFBR1 and modulating the TGF-β signaling pathway

Liyuan Ke [a,1], Ziyao Zheng [a,1], Shumin Ye [a,1], Chenhui Zhong [a], Qingyun Lin [a], Yan Hu [b], Peiying Shi [c,*], Lei Wen [d,*], Hong Yao [a,e,*]

[a] Department of Pharmaceutical Analysis, School of Pharmacy, Fujian Medical University, Fuzhou 350122, China
[b] Public Technology Service Center, Fujian Medical University, Fuzhou 350122, China
[c] Department of Traditional Chinese Medicine Resource and Development, College of Bee Science and Biomedicine, Fujian Agriculture and Forestry University, Fuzhou 350002, China
[d] The First Affiliated Hospital of Zhejiang Chinese Medical University (Zhejiang Provincial Hospital of Chinese Medicine), Hangzhou 310006, China
[e] Fujian Key Laboratory of Drug Target Discovery and Structural and Functional Research, Fujian Medical University, Fuzhou, 350122, China

ARTICLE INFO

Keywords:
Tanshinone I
Myocardial ischemia
Myocardial fibrosis
TGF-β signaling pathway
TGFBR1

ABSTRACT

Background: Tanshinone I (Tan I) is an essential active ingredient of the traditional cardiovascular medicine *Salvia miltiorrhiza* Bunge (*S. miltiorrhiza*). Although the protection of Tan I on cardiomyocyte has been reported, its anti-myocardial ischemia effects and mechanisms remain unknown.

Purpose: Systematic evaluation of the role of Tan I in reducing myocardial ischemia (MI) injury and elucidation of the underlying molecular mechanisms by which Tan I improves myocardial fibrosis and ventricular function in mouse MI models.

Methods: In vivo and *in vitro* MI models were constructed to substantiate the anti-MI effects of Tan I. Through target fishing, molecular docking, and network pharmacology investigation, the effect mechanisms and potential target proteins of Tan I against MI were predicted further. Tandem mass tags (TMT)-based quantitative proteomics, transforming growth factor beta receptor I (TGFBR1)-overexpressing lentiviral vectors, molecular dynamics (MD) simulations, biolayer interferometry (BLI), cellular thermal shift assay (CETSA), TGFBR1 kinase activity, and drug affinity responsive target stability (DARTS) assay were subsequently used to validate the anti-MI-effect mechanisms and targets of Tan I.

Results: Tan I can markedly increase the survival of oxidative stress cell models, improve intracellular environment, and inhibit the release of intracellular reactive oxygen species. Moreover, it can restore abnormal electrocardiograms, decrease myocardial infarction area, inhibit cardiac fibrosis, and reduce serum levels of key cardiac injury biomarkers in the MI mouse model. Mechanistically, Tan I considerably inhibited the phosphorylation modification levels of TGFBR1 and Smad2 and the aberrant expressions of Collagen I/III, α-smooth muscle actin, Bcl-2, and Bax proteins in MI mice. These findings were further verified in NIH-3T3 cells overexpressing TGFBR1 or activated by TGF-β1. MD simulations, CETSA, and DARTS showed that TGFBR1 binding to Tan I was relatively stable. In addition, BLI indicated that the equilibrium dissociation constant of Tan I binding TGFBR1 was 1.5×10^{-6} M. Based on the kinase activity assay, Tan I restrained TGFBR1 with a half-maximal inhibitory concentration of 739.6 nM.

Conclusion: This work reveals for the first time that Tan I can reduce MI injury and fibrosis by modulating the TGF-β signaling pathway via targeting of TGFBR1.

Abbreviations: BLI, biolayer interferometry; BP, Biological processes; BW, Body weight; CAP, Captopril; CC, Cellular components; CETSA, Cellular thermal shift assay; CK, Creatine kinase; CMC—Na, Carboxymethyl Cellulose Sodium; DARTS, drug affinity responsive target stability; DEPs, Differentially expressed proteins; DO, Disease Ontology; FBS, Fetal bovine serum; GO, Gene Ontology; HW, Heart weight; IF, Immunofluorescence; IHC, Immunohistochemistry; ISO, Isoprenaline Hydrochloride; KD, equilibrium dissociation constant; LADL, Ligation of the left anterior descending branch of the coronary artery; LV-GFP, Green fluorescent protein lentivirus; LV-TGFBR1, Lentiviral mouse TGFBR1; MD, Molecular dynamic; MF, Molecular functions; MCF, myocardial fibrosis; MI, Myocardial ischemia; NAC, N-Acetyl-L-Cysteine; PSR, Picro-sirius red; RLU, Luminescence; *S. miltiorrhiza*, *Salvia miltiorrhiza* Bunge; Tan I, Tanshinone I; t-BHP, Tert-Butyl hydroperoxide.

* Corresponding authors.
E-mail addresses: peiyshi@126.com, peiyshi@fafu.edu.cn (P. Shi), wenlei@zcmu.edu.cn (L. Wen), hongyao@mail.fjmu.edu.cn (H. Yao).
[1] These authors contributed equally to this work.

https://doi.org/10.1016/j.phymed.2025.156994
Received 24 January 2025; Received in revised form 24 April 2025; Accepted 16 June 2025
Available online 16 June 2025

Introduction

Cardiovascular diseases (CVDs) currently serve as the leading causes of noninfectious disease deaths worldwide, with ischemic heart disease being the most prevalent (Han et al., 2024; Velmurugan et al., 2020). Myocardial ischemia (MI) triggers a series of inflammatory responses, exacerbates the apoptosis and necrosis of cardiomyocytes, promotes cardiac fibroblasts and extracellular matrix (ECM) accumulation, and induces ventricular remodeling, which ultimately lead to severe cardiac dysfunction and heart failure (Anzai et al., 2017). Drug intervention is an effective means to combat MI. Hotspots of current research include screening of emerging anti-MI drugs and elucidation of their targets of action.

Salvia miltiorrhiza Bunge (*S. miltiorrhiza*) (Fig. 1A), is one of traditional medicines applied against CVDs, and it has been used clinically for more than thousands of years (Chen et al., 2019). *S. miltiorrhiza* possesses therapeutic activities, referring to anti-oxidant, anti-inflammatory, anti-fibrosis, and anti-cancer effects (Ke et al., 2023). Tanshinone I (Tan I) represents an important active ingredient in *S. miltiorrhiza*. Tan I can inhibit the RIP1/RIP3/MLKL pathway, promote the transcription and expression of Nrf2, inhibit the mitogen-activated protein kinase signaling pathway (Wu et al., 2021), block IGF-1R/PI3K signaling (Wu et al., 2019), and exert cardiomyocyte protective effects. Therefore, Tan I possesses potential in the therapeutic area of CVDs, *e.g.*, as an anti-MI agent. However, thus far, the anti-MI effects and mechanisms of Tan I have not been reported, which is unfavorable to the subsequent research and application of the active ingredient or compound preparations containing *S. miltiorrhiza*.

The transforming growth factor-β (TGF-β) signaling pathway plays a pivotal role in the fibrotic process in a variety of tissues, particularly in the progression of myocardial fibrosis (MCF) due to MI (Edsfeldt et al., 2023). TGF-β signaling pathway involves the binding of TGF-β1, a secreted cytokine, to TGF-β receptor II (TGFBR2), which in turn triggers the activation and phosphorylation of TGFBR1. This process subsequently results in the phosphorylation of Smad2/3, which combines with Smad4 to form a complex whose subsequent entry into the nucleus triggers an array of transcriptional events, including the promotion of fibroblast proliferation and activation, enhancement of collagen production, and resultant aberrant accumulation of the ECM, which ultimately cause MCF and induce ventricular remodeling (Travers et al., 2022). Given that *S. miltiorrhiza* ethanol extract (SMEE) can substantially alleviate chronic renal failure via the regulation of TGF-β/Smad signaling pathways (Xiang et al., 2019), Tan I, as one of the main active ingredients of SMEE, also possibly regulates the TGF-β/Smad signaling pathway to exert anti-MCF effects.

In a word, the therapeutic effects and underlying mechanisms of Tan I against MI and MCF require further elucidation. In view of this, this study aimed to determine the therapeutic properties and reveal the potential mechanisms of Tan I through *in vivo* and *in vitro* MI and MCF modeling using network pharmacology, proteomics, gene editing, molecular dynamics (MD) simulation, cellular thermal shift assay (CETSA), drug affinity responsive target stability (DARTS), biolayer interferometry (BLI), and TGFBR1 kinase activity assays.

Materials and methods

Chemical and reagents

Tan I (B20256) was provided by Shanghai yuanye Bio-Technology Co. Ltd. (Shanghai, China), and its purity (≥98 %) was determined via HPLC (Fig. 1A). TGFBR1 (A0708) antibody was purchased from ABclonal (Wuhan, China). Phosphorylated-TGFBR1 (PA5–40,298) antibody was obtained from Invitrogen (Waltham, MA, USA). Information on other chemicals and reagents can be found in Supplementary Materials.

Animal-based pharmacodynamic assays

Male ICR mice (6–8 weeks old, 20–25 g), were provided by the Animal Center of Fujian Medical University with standardized care. Procedures for animal care and experiments were approved by the Animal Ethics Committee of Fujian Medical University (IACUC FJMU 2023–0126; Date: June 1, 2023).

Mouse model establishment

An acute MI mouse model was produced through ligating the left anterior descending branch of the coronary artery (LADL) (Gao et al., 2010). Briefly, the mice were anesthetized with 50 mg/kg sodium pentobarbital (*i.p.*) and maintained on small-animal ventilators after being secured by tape in a supine position. A small transverse incision was performed at the third and fourth intercostal space on the left side of the mouse sternum, followed by separation of muscles to expose the heart. The left anterior descending coronary artery was ligated with a 6–0 surgical thread, which resulted in rapid ischemic whitening of left ventricular anterior wall, as well as ST-segment elevation on the electrocardiogram, confirming the effectiveness of the ligation. The surgical steps of the sham mice were consistent with those of the experimental group except that no ligation operation was performed.

A chronic MI mouse model was also constructed through subcutaneous injection of ISO at a dose of 5 mg/kg/day for 21 days (Eladwy et al., 2018).

Animal administration

For acute MI animal experiments, 72 healthy male mice were randomized into six different experimental groups: Sham, LADL, Tan I (1, 3, and 5 mg/kg/day, *i.g.*), and captopril (CAP) groups (15 mg/kg/day, *i.g.*). The solvent was 0.5 % CMC—Na. Three days before surgery, the Sham and model groups were given 0.5 % CMC—Na (*i.g.*), and the Tan I and CAP groups were given Tan I and CAP at the designed doses, respectively. Postoperatively, the same treatment was continued for 5 days in the surviving mice.

For chronic MI animal experiments, 72 healthy male mice were also randomized into six groups including control, ISO (5 mg/kg/day, *s.c.*), Tan I (1, 3, and 5 mg/kg/day, *i.g.*), and CAP groups (15 mg/kg/day, *i.g.*). The control and ISO groups were given 0.5 % CMC—Na via tail vein once per day, and the other groups were injected Tan I and CAP for three days of preprotection at the designed doses. After three days, ISO in normal saline was injected subcutaneously for 21 days except for the control group, and the same drug treatment was continued for the mice.

Electrocardiography (ECG)

Mice were anesthetized with sodium pentobarbital (50 mg/kg, *i.p.*), fixed in supine position on a fixator and connected to an MD3000 Bio-Signal Acquisition System (Anhui Zhenghua Biologic Apparatus Facilities Limited Company, Huaibei, China), in accordance with the instruction manual. The electrocardiograms of the mice were then detected and recorded for 30 s to 2 min.

General observations on mice

The general condition of the mice was observed and recorded daily. At the end of the experiment, the mice were euthanized (carbon dioxide overdose anesthesia), and serum and hearts were collected for subsequent analysis.

Histological staining

Heart tissues were dehydrated and embedded after immobilization in 4 % paraformaldehyde and then serially sectioned at a thickness of 1.0 mm. Subsequently, hematoxylin and eosin (H&E) staining was carried out according to the instructions provided by the manufacturer. Meanwhile, MCF was assessed through Picro-sirius red (PSR) and Masson's trichrome staining. The images were then captured using a fluorescence microscope (NIKON Eclipse Ci, Tokyo, Japan) and analyzed with ImageJ

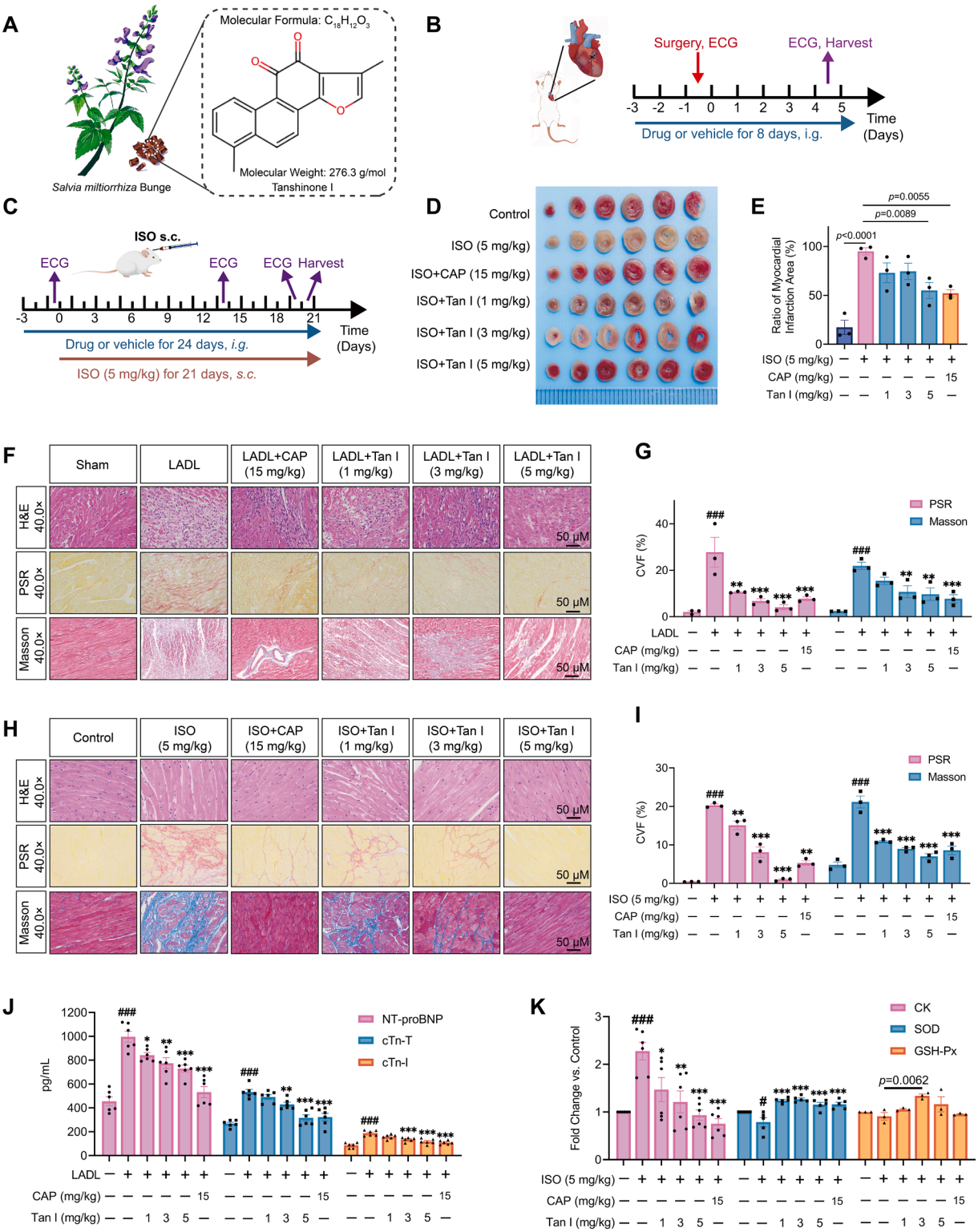

Fig. 1. Tan I improved acute and chronic myocardial ischemic injury. (A) Morphology of *Salvia miltiorrhiza* Bunge (*S. miltiorrhiza,* left) and structural formula of Tanshinone I (Tan I, right). (B) Schematic timeline of animal experiments for the LADL model: Tan I (1,3,5 mg/kg/day, *i.g.*) was given continuously for 8 days, LADL surgery was performed on the third day of treatment, and the mice were executed 5 days after surgery. (C) Schematic timeline of animal experiments in the ISO model: Tan I (1,3,5 mg/kg/day, *i.g.*) was given continuously for 24 days, and ISO (5 mg/kg/day, *s.c.*) was given concurrently on the third day of treatment for 3 weeks, and the mice were executed 21 days after subcutaneous injection. (D, E) Representative images of TTC and calculated infarcted size of the myocardium ($n = 3$). (F) Representative H&E, PSR, and Masson trichrome-stained images of cardiac tissue from each group of mice in the LADL model at 40× (scale bar = 50 μm) lens. (G) Collagen volume fraction (CVF) of PSR and Masson trichrome staining in each group of mice in the LADL model ($n = 3$). (H) Representative H&E, PSR, and Masson trichrome-stained images of cardiac tissue from each group of mice in the ISO model at 40× (scale bar = 50 μm) lens. (I) CVF of PSR and Masson trichrome staining in each group of mice in the ISO model ($n = 3$). (J) Content of NT-proBNP, cTn-I, and cTn-T in the serum of mice in each group of the LADL model ($n = 6$). (K) Activities of CK, total SOD and GSH-Px in the serum of mice from each group of the ISO model ($n = 6$). Data are expressed as mean ± SEM, $\#p < 0.05$, and $^{\#\#\#}p < 0.001$ *versus* sham or control group; $^{*}p < 0.05$, $^{**}p < 0.01$, and $^{***}p < 0.001$ *versus* LADL or ISO group.

version 1.53e (MD, USA).

Assessment of myocardial infarct size

As previously described (Lee et al., 2021), myocardial infarcted areas were detected via 2,3,5-triphenyltetrazolium chloride (TTC) staining. Briefly, at the end of the experiment, hearts were removed and rapidly frozen at -80 °C, retrieved, and cut into six 1 mm slices equidistant from below the ligation point. Then, they were incubated in phosphate-buffered 1 % TTC solution at 37 °C for 10 min. Undamaged myocardium appeared red, whereas infarcted tissues remained pale. Images were recorded using a digital camera (Canon, Tokyo, Japan), and infarcted areas were quantitatively analyzed using ImageJ software.

Serum biochemical index detection

Blood samples were collected from each mouse later stage in the experiment, and then centrifuged at 3000 rpm for 15 min at a temperature of 2−8 °C to separate the serum of each sample.

Following the manufacturer's guidelines, cardiac troponin (cTn)-T, cTn-I, and N-terminal pro-B-type natriuretic peptide proteins (NT-proBNP) were assayed in mouse serum using enzyme-linked immunosorbent assay (ELISA) kits supplied by Jiangsu Sumeike Biological Technology Co., Ltd. (Jiangsu, China).

Chronic MI mouse groups were assayed for glutathione peroxidase (GSH-Px) (A005) and superoxide dismutase (SOD) (A001–1) levels using the kits from Nanjing Jiancheng Bioengineering Institute (Nanjing, China), and creatine kinase (CK) indexes were determined using the kits (S03024) received from Rayto Life and Analytical Sciences Co., Ltd. (Shenzhen, China), following the manufacturer's instructions.

Cell-based pharmacodynamics experiments

H9c2 rat cardiomyocytes, AC16 human cardiomyocytes, and NIH-3T3 mouse embryonic fibroblasts were acquired from the Wuhan Pricella Biotechnology Co., Ltd. (Wuhan, China). For detailed information on methods and procedures, please see the supplementary information.

Oxidative stress model

H9c2 and AC16 cells were inoculated at a density of 5.0×10^3 cells/well in 96-well plates and cultured to 80 % confluence. After 24 h of H9c2 serum starvation in serum-free Dulbecco's Modified Eagle Medium (DMEM) diluted with 0.1 % DMSO, the original culture solution was aspirated and discarded, and 100 μl t-BHP solution with a series of concentration was added, which resulted in the final concentrations of 0, 100, 200, 300, and 400 μM, followed by 2 h incubation. For AC16 cells, the operation was the same as those for H9c2 cells, except that the final concentrations of t-BHP were 1, 2, 3, 4, 5, 6, 7, 8, and 9 mM. Cell viability was detected through 3-[4,5-dimethylthiazol-2-yl]-2,5 diphenyl tetrazolium bromide (MTT) assay, with the absorbance measured at 490 or 570 nm (Li et al., 2022), and the appropriate concentration of t-BHP was screened for constructing an oxidative stress model for H9c2 and AC16 cells.

Cell viability assays

When both cell densities reach the required level, a series of concentrations of 100 μl Tan I solutions (containing 0.1 % DMSO serum-free DMEM solution as solvent) were added to the wells, resulting in a final Tan I concentration of 0, 0.01, 0.1, 0.5, 1, 1.25, 2.5, or 5 μM for 24 h treatment. MTT assay was used to assess the effect of Tan I on the growth of H9c2 and AC16 cells.

For *in vitro* oxidative damage experiments. When both cell densities reach the required level, a series concentrations of Tan I solutions was added to the wells with a final concentration of 0, 0.01, 0.05, 0.1, 0.5, or 1 μM in serum-free DMEM containing 0.1 % DMSO, and 400 μM NAC as positive control (Zhao et al., 2017); the medium was aspirated and discarded after 4, 12, and 24 h of pretreatment. Afterward, oxidative damage was induced through the addition of the corresponding gradient concentration of Tan I and 200 μM (H9c2) or 3 mM (AC16) t-BHP. Cell viability was measured via the MTT method to analyze the protective effect of Tan I against t-BHP-induced oxidative stress injury in H9c2 and AC16 cells.

Determination of intracellular reactive oxygen species (ROS) content

H9c2 or AC16 cells were treated with 10 μM dichlorofluorescein diacetate (DCFH-DA) at 37 °C for 30 min, followed by three washes with phosphate buffered saline. The ROS levels in H9c2 and AC16 cells were observed through fluorescence microscopy (Leica, Wetzlar, Germany).

Network pharmacology and molecular docking

Prediction for the targets of Tan I

Tan I structure was searched and saved in a SDF file from PubChem (https://pubchem.ncbi.nlm.nih.gov/). The structure was imported into PharmMapper database (http://lilab-ecust.cn/pharmmapper/index.html), the human source database was defined, and target fishing and prediction were performed (Gao et al., 2021).

Prediction of potential targets of Tan I against MI

Target proteins related to "myocardial ischemia" (containing "myocardial fibrosis") were searched in OMIM (https://www.omim.org/) and GeneCards (https://www.genecards.org/) databases, and were integrated to exclude duplicates (Zhu et al., 2020). Comprehensive drug and disease target database analysis was performed to identify the potential targets for Tan I against MI and MCF. Eventually, the predicted target proteins were loaded into UniProt database (https://www.uniprot.org/) to obtain their official symbols, with the species defined as "human" (Zhong et al., 2025).

Bioinformatics analysis for potential targets of Tan I against MI

The R language packages "clusterProfiler," "org.Hs.eg.db," "topGO," and "DOSE" were used to perform Gene Ontology (GO) enrichment analysis, Kyoto Encyclopedia of Genes and Genomes (KEGG) pathway enrichment analysis and Disease Ontology (DO) enrichment analysis, followed by protein–protein interaction analysis using STRING database (https://cn.string-db.org/) and component-target-disease network construction using Cytoscape 3.9.1 software (Francis et al., 2024; Qu et al., 2023).

Molecular docking of potential targets of Tan I against MI

The affinity and binding free energies of Tan I to potential target proteins were predicted using Sybyl-X 1.3 software, and their binding was visualized using PyMOL 2.3.1 software (Zhong et al., 2025; Zhou et al., 2023).

TMT-based quantitative proteomics

According to a previous report, TMT-based quantitative proteomics analysis was conducted (Xie et al., 2024). 1 μM Tan I was used to intervene in the H9c2 cardiomyocyte damage caused by t-BHP (200 μM). In the experiments, control, model, and Tan I-treated groups were set up with three independent replications for each group. The collected cell precipitates were digested and liquid chromatography tandem mass spectrometry analysis was used to identify proteins for the control, model and Tan I groups (see Supplementary Information).

The enrichment ratio of differentially expressed proteins (DEPs) to the total identified proteins was assessed through a two-tailed Fisher's exact test. KEGG pathway analyses applying a two-tailed Fisher's exact test were also performed to identify the enrichment of DEPs. GO annotation were categorized into three main groups referring to biological processes (BP), cellular components (CC) and molecular functions (MF). GO or KEGG pathway with a corrected P-value < 0.05 was determined to be significant (Table S1).

Real-time PCR (QPCR)

As mentioned in previous studies (Kalyanaraman et al., 2024), total RNA was extracted using the Rapid Animal Tissue/Cell Total RNA Extraction Kit (Servicebio, Wuhan, China). RNA was then reverse transcribed to cDNA using SweScript All-in-One RT SuperMix for quantitative polymerase chain reaction (qPCR) (Servicebio, Wuhan, China). qPCR was conducted with 2×Universal Blue SYBR Green qPCR Master (Servicebio, Wuhan, China). The mRNA levels were normalized to the average expression levels of GAPDH or β-tubulin. Table S2 shows the sequences of primers.

Western blot (WB)

WB experiments were performed as previously described (Bai et al., 2023). Details on the methods and procedures are provided in Supplementary Information.

Immunohistochemistry (IHC)

Heart tissues from the ISO-induced MI model were obtained. See supplementary information for details on methods and procedures.

Immunofluorescence (IF)

Cell samples were experimented based on NIH-3T3. Supplementary Information provide on details on methods and procedures.

Overexpression (OE) of TGFBR1 and agonist or antagonist competition assay

Lentiviral mouse TGFBR1 (LV-TGFBR1)-overexpressing and enhanced green fluorescent protein lentivirus were obtained using Jingruibio Biotechnology Co., Ltd (Guangdong, China) Lentivirus Packaging Kit (L002C). NIH-3T3 cells were infected in serum-free DMEM with the multiplicity of infection (MOI) of 100 for 6 h, and then complete DMEM were added. After 48 h, cell morphology and fluorescence were observed under a fluorescence microscope (Leica, Wetzlar, Germany).

After screening with puromycin for 7 days, NIH-3T3 cells infected with LV-TGFBR1 were harvested, and they were OE positive. Subsequently, the cell culture medium was replaced with a fresh one, followed by treatment with TGF-β1 (10 ng/ml) as an activator of TGFBR1 for 24 h or with the inhibitor A83–01 (1 μM) for 12 h. Subsequently, to detect the expression of relevant proteins, we collected NIH-3T3 and performed WB and IF analysis.

MD simulation

MD simulation followed the approach of previous reports (Krishnasamy et al., 2024; Zhong et al., 2025). Briefly, we obtained the complex structure of Tan I or A83–01 with TGFBR1 proteins via the AutoDock 4.2.6 software and used it as a starting point for 50 ns for whole-atom MD simulations using GROMACS 2024.2 software. The protein model was constructed based on the amber ff14SB force field, and the small molecule was set on the general amber force field. The simulation box had fixed dimensions set to ensure that each atom of the protein was >1.0 nm away from the box edge. All simulations were run with periodic boundary conditions on the NVT set and the temperature was held at 310 K and the pressure at 1 atm. The dynamic stability of the proteins and complexes within the system was assessed through the analysis of the root mean square deviation (RMSD), root mean square fluctuation (RMSF), and Gibbs energy landscape within 50 ns.

BLI analysis

The affinity of Tan I to the target protein TGFBR1 was characterized using the fortéBIO Octet RED 96 system. TGFBR1 protein (Sino Biological Inc., Beijing, China) was immobilized to Super streptavidin biosensors (Pall fortéBIO Corp, Menlo Park, *CA*). Different concentrations of Tan I were used to test binding, which was performed using fortéBIO data analysis software. The binding curves were fitted using global fitting and 1:1 modeling to determine equilibrium dissociation constants (KD).

CETSA

CETSA was conducted in accordance with a previous report (Yang et al., 2023). NIH-3T3 cells were pretreated with Tan I (0.1 μM) for 12 h as the Tan I-treated group, and the solvent control and Tan I-treated cells were equally divided into nine groups and heated at different temperatures (25 °C; 37 °C–72 °C, 5 °C intervals). After heating the cells for 3 min at the indicated temperatures, they were lysed using liquid nitrogen via the freeze-thaw method. Afterward, the cell supernatants were collected through centrifugation, added to protein super sampling buffer, and then boiled for 5 min for WB analysis.

TGFBR1 kinase activity assay

TGFBR1 kinase activity was determined using the ADP-Glo Kinase Assay and TGFβR1 Kinase Enzyme System kit (Promega, Beijing, China). Briefly, Tan I was diluted from 10^5 nM to $10^5/2^{11}$ nM in a gradient of 12 groups. Then, 1 μl of the indicated concentrations of Tan I, 2 μl TGFBR1 kinase (12.5 ng/μl), 1 μl ATP (250 μM), and 1 μl TGFBR1 substrate (1 μg/μl) were added to 384-well plates, and the plates were incubated for 2 h at room temperature. Subsequently, the reaction was stopped by supplementing 5 μl ADP-Glo™ reagent, and the remaining ATP was consumed by incubation for 40 min. Finally, the reaction was supplemented with 10 μl kinase detection reagent, and after incubation for 30 min, luminescence was recorded using a SpectraMax iD3 multifunctional microtiter plate reader. The half-maximal inhibitory concentration (IC_{50}) of Tan I was calculated using GraphPad Prism 8.0.

DARTS

DARTS experiment was performed in accordance with previous studies (Deng et al., 2025), and cardiomyocytes were fully lysed on ice using NP-40 buffer. Then, the cardiomyocytes were incubated with Tan I or DMSO for 1 h at 37 °C, mixed with pronase E (MedChemExpress, New Jersey, USA) at a 500:1 ratio, and analyzed by WB.

Statistical analysis

The experimental data are expressed as mean ± standard error of the mean (SEM) of at least three independent experiments and were analyzed using Microsoft Excel 2010. Comparisons between two groups were performed using unpaired *t*-tests. In other cases, significance across more than two groups was determined through with one-way analysis of variance. The difference was considered statistically significant when $p < 0.05$.

Results

Tan I protects the heart from ischemic damage

The intervention effect of Tan I on MI was first investigated in two MI mouse models. Fig. 1B shows the schematic timeline of the experiments on the animals of the LADL model group, and Fig. 1C displays the subcutaneous injection of the ISO model group. The results reveal that the ST-segment elevation in ECGs of the LADL model group was evident

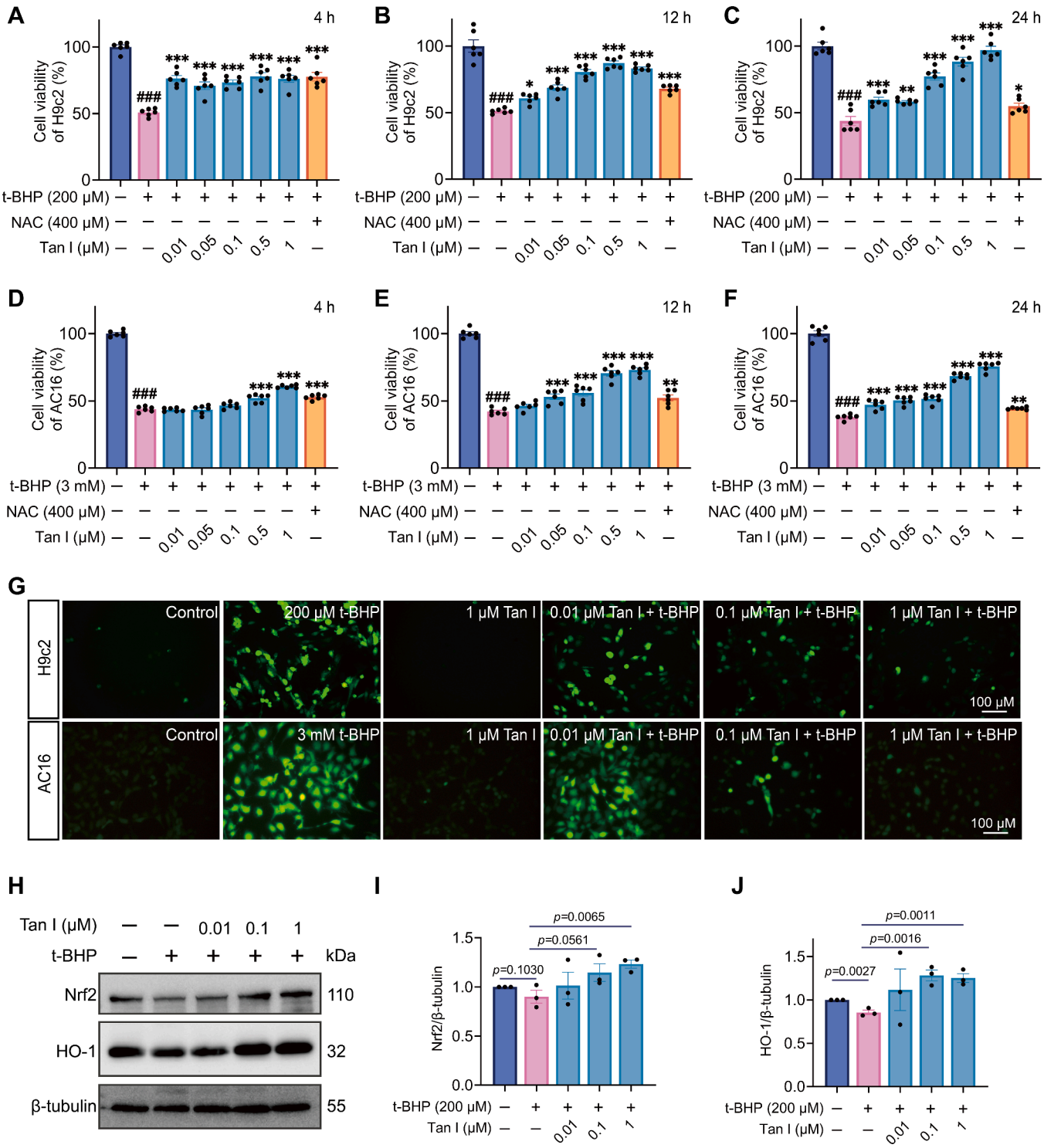

Fig. 2. Tan I ameliorates oxidative stress induced by t-BHP in cardiomyocytes. (A–C) MTT assay for H9c2 cardiomyocyte viability. Effect of Tan I pretreatment for 4 h,12 h and 24 h on t-BHP (200 μM) induced oxidative stress in cells ($n = 6$). (D–F) MTT assay for AC16 cardiomyocyte viability. Effect of Tan I pretreatment for 4 h,12 h and 24 h on t-BHP (3 mM) induced oxidative stress in cells ($n = 6$). (G) Representative images of DCFH-DA staining in H9c2 and AC16 (scale bar = 100 μm). (H, I) The effects of Tan I treatment on t-BHP-induced Nrf2, and HO-1 protein expression in H9c2 cells and quantified using Image Lab software ($n = 3$). Data are expressed as mean ± SEM, ###$p < 0.001$ *versus* control group; *$p < 0.05$, **$p < 0.01$, and ***$p < 0.001$ *versus* t-BHP group.

along with the attenuated R-wave amplitude and the development of pathologic Q waves. Meanwhile, the degree of ST-segment elevation was moderated and abnormal ECGs were improved in Tan I pretreated and treated mice (Fig. S1A). In addition, ST-segment inversion or elevation of the ECG can be monitored on days 14 and 20 in mice from each group of ISO (5 mg/kg, *s.c.*)-induced MI and MCF, and the ECGs of the Tan I-pretreated and treated mice exhibited trend recovery (Fig. S1B). In addition, as the ISO induction days increased, the mice in the ISO model group showed severe appetite loss, remarkable weight loss, decreased locomotor activity, disheveled and rough fur, and grayish skin color on the tail. Notably, the Tan I and CAP groups displayed more vigor than the ISO model group, with notably higher appetite, slight weight loss,

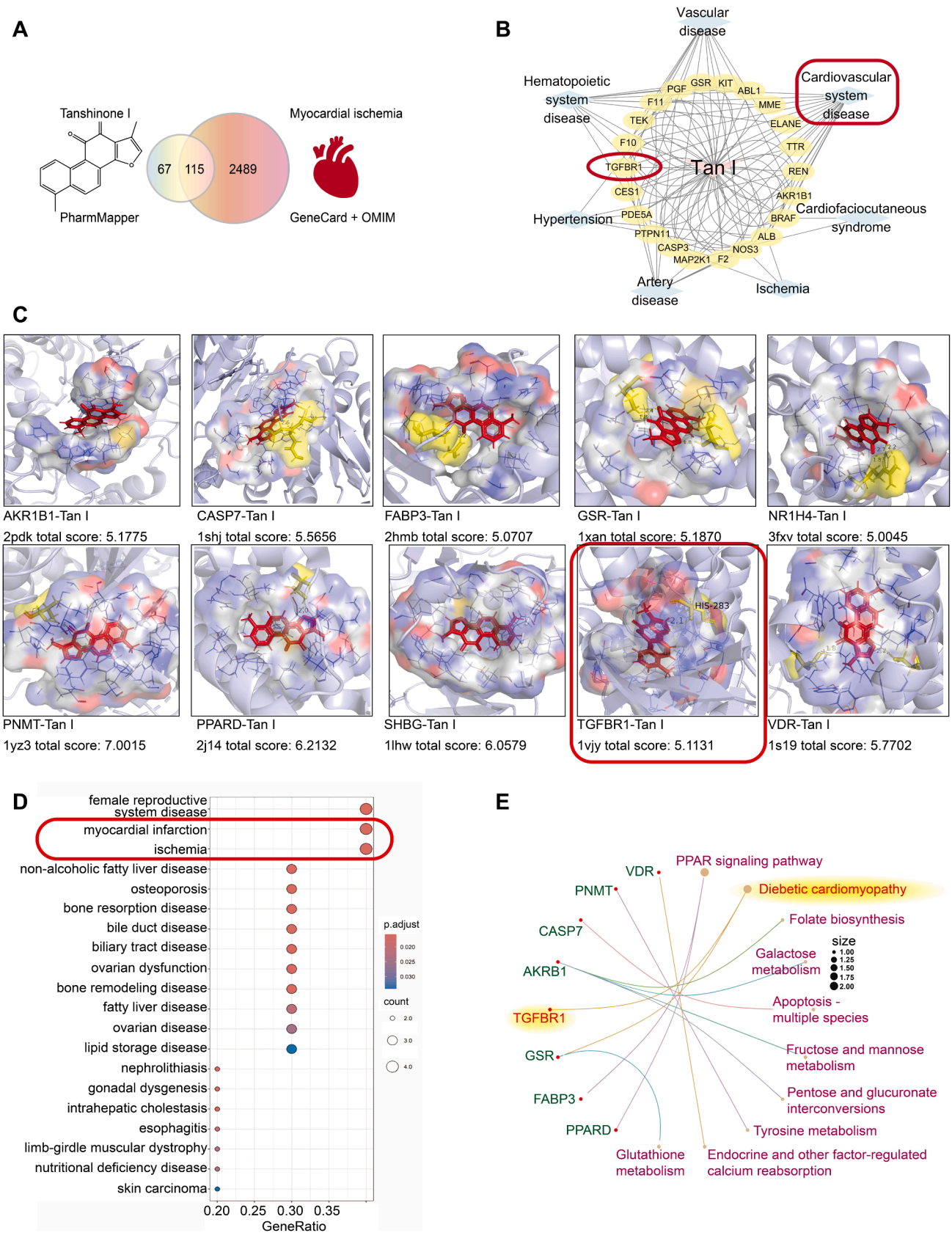

Fig. 3. Screening and bioinformatics analysis of anti-MI targets associated to Tan I. (A) Intersection of virtual screening target proteins of Tan I with myocardial ischemia disease-associated proteins Venn diagram. (B) "Component-Disease-Target" network diagram for Tan I related to cardiovascular disease. (C) PyMol visualization of 10 highly scored potential target proteins obtained by docking with Tan I molecules. (D) Dotplot of DO enrichment analysis of 10 potential target proteins. The circle color indicates the enrichment significance *P* value, and the circle size indicates the number of differential proteins in the functional class or pathway. (E) Cnet plot of KEGG enrichment for 10 potential target proteins. Larger circles indicate a higher relative ratio of the number of proteins enriched.

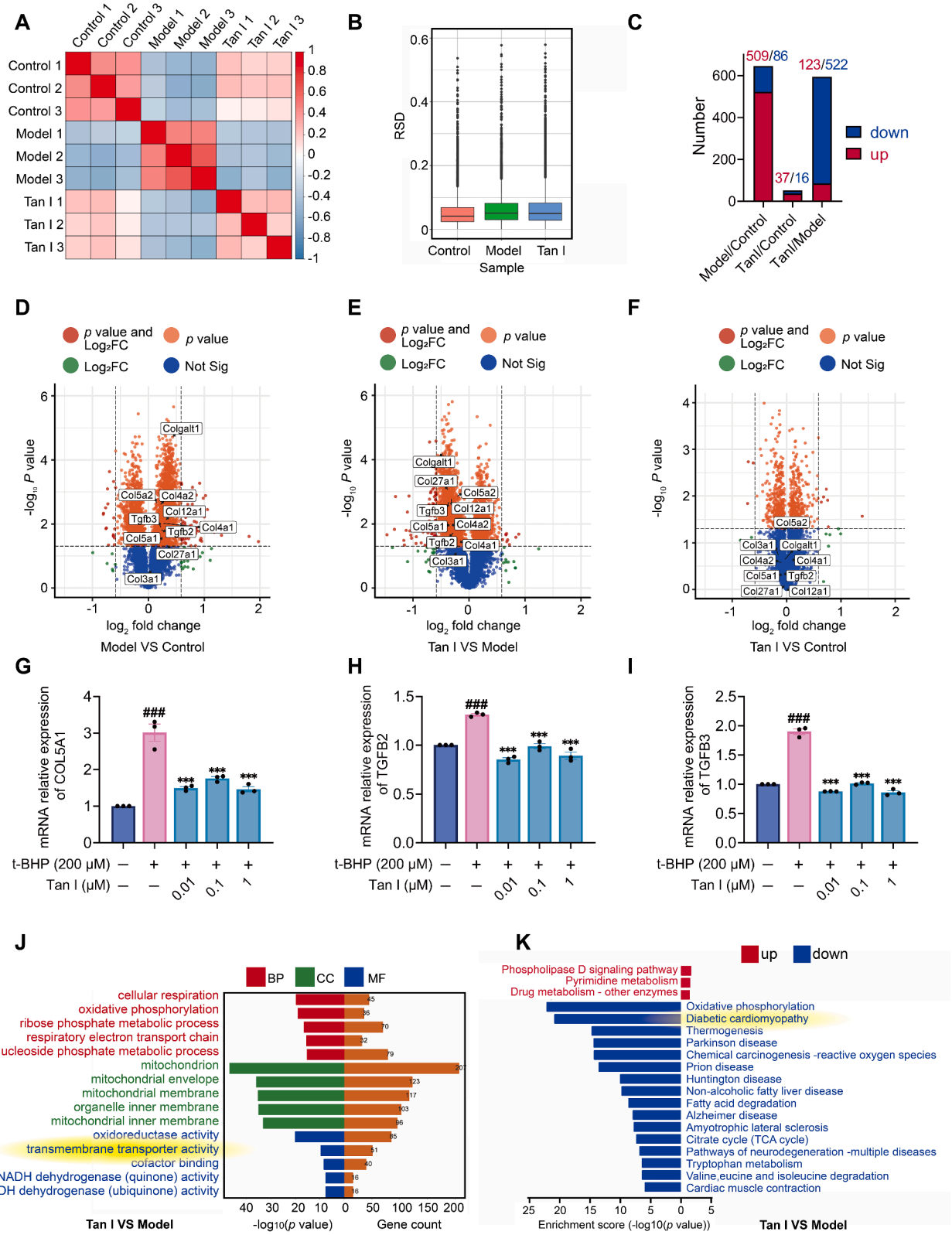

Fig. 4. TMT-based quantitative proteomic analysis for t-BHP-induced damage in H9c2 cardiomyocytes by Tan I intervention. (A) Heatmap of the PCC between two of the three sample groups. PCC values close to -1 are negatively correlated, close to 1 are positively correlated, and close to 0 are uncorrelated. (B) Box line plot of RSD of protein quantification values between three sets of replicate samples. The overall RSD values were below 0.1, with excellent quantitative reproducibility. (C) Statistical chart of differential proteins between the three groups. (D) Volcano plots of differential proteins about the model and control groups. (E) Volcano plots of differential proteins about the Tan I and model groups. (F) Volcano plots of differential proteins about the Tan I and control groups. (G–I) Inhibitory effect of Tan I on COL5A1, TGFB2 and TGFB3 mRNA expression levels in H9c2 cells stimulated with t-BHP. Comparison with the mean expression levels of GAPDH and β-Tubulin, $n = 3$. (J, K) Bar charts of the enrichment analysis of GO and KEGG pathway for differential proteins between Tan I and model groups. Data are expressed as mean ± SEM, $###p < 0.001$ *versus* control group; $***p < 0.001$ *versus* t-BHP group.

and normal defecation. Especially, the high-concentration Tan I group had neat and straight hair and pinkish tail color (Fig. S1C). It demonstrated that Tan I can promote the recovery of ischemic myocardial function with cardioprotective effect. Afterwards, the mouse heart weight (HW) and body weight (BW) were determined, and the results show that the HW/BW ratio decreased after Tan I or CAP pretreatment and treatment in the LADL (Fig. S1D) and ISO (Figs. S1E and S1F) model assays. These findings imply that Tan I ameliorated cardiac hypertrophy and alleviated the increase in cardiac heavy load. Mouse hearts were collected to detect the myocardial infarct area through TTC staining. The results unveil that the infarct area reached >90 % after 21 days of ISO induction, and 5 mg/kg Tan I pre-treatment and treatment significantly reduced the myocardial infarct area of MI mice (F (5, 12) =13.20, p = 0.0089) (Figs. 1D and 1E).

To evaluate the extent of MI and MCF, we stained the cardiac paraffin sections with H&E, PSR, or Masson's trichrome. As results, the mice in the LADL (Figs. 1F and1 G) or ISO model group (Figs. 1H and 1I) had ruptured cardiomyocytes or loss of cytomembranes, large amounts of collagen deposition or diffusion, and increased interstitial fibrosis. Meanwhile, cardiomyocytes in the mice pretreated and treated with Tan I or CAP were relatively neatly aligned, with mild widening of a portion of the interstitial edema and markedly reduced levels of collagen fibers. The anti-MCF effect of Tan I at 5 mg/kg was partially superior to that of the CAP group. Next, we measured NT-proBNP (F (5, 30) =26.6, p < 0.0001), cTn-T (F (5, 30) = 23.46, p < 0.0001), and cTn-I (F (5, 30) = 19.67, p < 0.0001) (Fig. 2J) in the mouse serum of each group. The findings indicate that LADL resulted in increased levels of these markers, and Tan I pretreatment and treatment reduced the levels of myocardial injury markers. Moreover, we examined the serum levels of CK (F (5, 30) = 9.191, p < 0.0001), SOD (F (5, 24) = 12.01, p < 0.0001), and GSH-Px (F (5, 12) = 4.522, p = 0.0150) (Fig. 1K) in ISO mouse model assays. The results reveal that Tan I intervention down-regulated the CK levels, contributed to the activation of the glutathione peroxidase system, and reversed the decrease in SOD levels induced by ISO.

The outcomes of the above *in vivo* experiments collectively support that Tan I pretreatment and treatment can effectively improve MI and MCF.

Tan I attenuates oxidative stress in cardiomyocytes

An oxidative stress model with rat H9c2 cardiomyocytes or human AC16 cardiomyocytes was constructed with t-BHP induction to further confirm the protective effects of Tan I on cardiac cells (Figs. S2A–S2D). Tan I pretreatment for 4, 12, and 24 h effectively ameliorated t-BHP-induced oxidative stress in H9c2 (Figs. 2A–2C) and AC16 cells (Figs. 2D–2F) in a concentration-dependent manner. Additionally, intracellular ROS levels, indicated by DCFH-Da intensity, were significantly increased by t-BHP stimulation in H9c2 and AC16 cells (Fig. 2G), and Tan I restored them to relatively normal levels in a concentration-dependent manner. Oxidative stress effector proteins were investigated to further determine the antioxidant capacity of Tan I. The protein levels of Nrf2, and HO-1 were significantly reduced in t-BHP-treated H9c2 cells compared with the control group, whereas they were up-regulated after Tan I intervention (Figs. 2H and I).

In conclusion, Tan I pretreatment can effectively ameliorate oxidative stress in cardiomyocytes and reduce the rate of apoptosis, consistent with the results of *in vivo* experiments.

Prediction of key target proteins of Tan I against MI

The target fishing web server PharmMapper was used to screen the possible target proteins of Tan I. Combined with the search for MI-related genes in the databases of OMIM and GeneCards, 115 potential target proteins of Tan I were screened by considering the intersections between the target fishing results and the proteins of the obtained MI-related genes for the anti-MI effects of Tan I (Fig. 3A). The 115 potential target proteins were imported into the STRING database for "component-disease-target" network analysis, and was visualized using Cytoscape software. Among these proteins, 22 targets, including TGFBR1, GSR, MAP2K1, CASP3, BRAF, etc. (Fig. 3B), were associated with CVDs, ischemia, arterial diseases, and other heart-related diseases. In addition, the potential proteins were used for molecular docking with Tan I to assess binding potential, and 10 highly rated (total score > 5) proteins containing TGFBR1 were obtained (Fig. 3C and Table S3). Interestingly, DO enrichment analysis results of these 10 high-scoring targets were mainly associated with myocardial infarction, ischemia, etc. (Fig. 3D). Meanwhile, KEGG pathway enrichment analysis revealed that the anti-MI mechanism of Tan I may be relevant to the potential target protein TGFBR1 and the diabetes cardiomyopathy pathway (Fig. 3E).

Proteomic analysis reveals that Tan I may target the TGFBR1 protein for TGF-β pathway signaling

To explore the underlying mechanism of Tan I against t-BHP-induced oxidative stress in cardiomyocytes, we performed proteomic analysis to screen differentially expressed proteins, followed by gene function analysis to identify potential pathway signals and functional targets. Supplementary Figs. S3A–S3E show the results of mass spectrometry database searches and data quality control results for the three groups of samples. To assess the reproducibility and reliability of the quantitative results of biologically duplicated or technically duplicated samples, we performed principal component analysis (PCA). The results suggest that no crossover of aggregation occurred between groups, and within-group samples displayed a good degree of aggregation (Fig. S3F). Using Pearson's correlation coefficient (PCC) analysis, the heatmap showed a high intragroup correlation among the three groups. However, the model group was negatively correlated with the Tan I and control groups, which exhibited a correlation but lower than the intra-group correlation (Fig. 4A). Meanwhile, the box line plots drawn using the relative standard deviation (RSD) of the quantitative values of protein between the duplicate samples of each group revealed that the RSD values of all three groups ranged from 0 to 0.1 (Fig. 4B). In summary, the protein samples of the control, model, and Tan I groups performed well in terms of intragroup reproducibility, and differences were observed among the three groups of samples, which satisfied the quality control criteria. The number of up-regulated proteins increased to 509 under t-BHP induction, and Tan I treatment resulted in the down-regulated expression of 522 proteins, which suggests that this outcome was likely to be due to the modulation of the differential protein expression by the post-Tan I treatment (Figs. 4C and S4A). The volcano plot results instructed that the capability to down-regulate the up-regulation of proteins associated with TGF-β pathway signaling (which belongs to diabetic cardiomyopathy pathway in KEGG pathway), such as collagen, resulted from t-BHP induction under Tan I treatment (Figs. 4D–4F). Thus, we further validated this finding at the gene transcription level (Figs. 4G–4I) and showed that Tan I can significantly down-regulate the transcript levels of COL5A1 (F (4, 10) = 34.48, p < 0.0001), TGFB2 (F (4, 10) = 44.50, p < 0.0001), and TGFB3 (F (4, 10) = 181.5, p < 0.0001). Consistently, intervention with Tan I suppressed the expression level of TGFB3 protein (F (2, 2) =1.491, p = 0.0431; Figs. S3G and S3H).

We performed bioinformatics analysis to further explore the relationship between the different differentially expressed proteins. The GO enrichment demonstrated that Tan I was involved in MF, such as oxidoreductase activity, and transmembrane transport activity (Figs. 4J and S4B–S4D). Meanwhile, the diabetic cardiomyopathy pathway (map 05,415, including the TGF-β signaling pathway) was definitely hit in the KEGG pathway enrichment analysis for Tan I intervention in H9c2 cardiomyocytes (Figs. 4K and S4E), which supports the predicted results of network pharmacology, that is, the anti-MI mechanism of Tan I is related to the diabetes cardiomyopathy pathway and TGFBR1 protein. Therefore, based on the results of proteomics and network

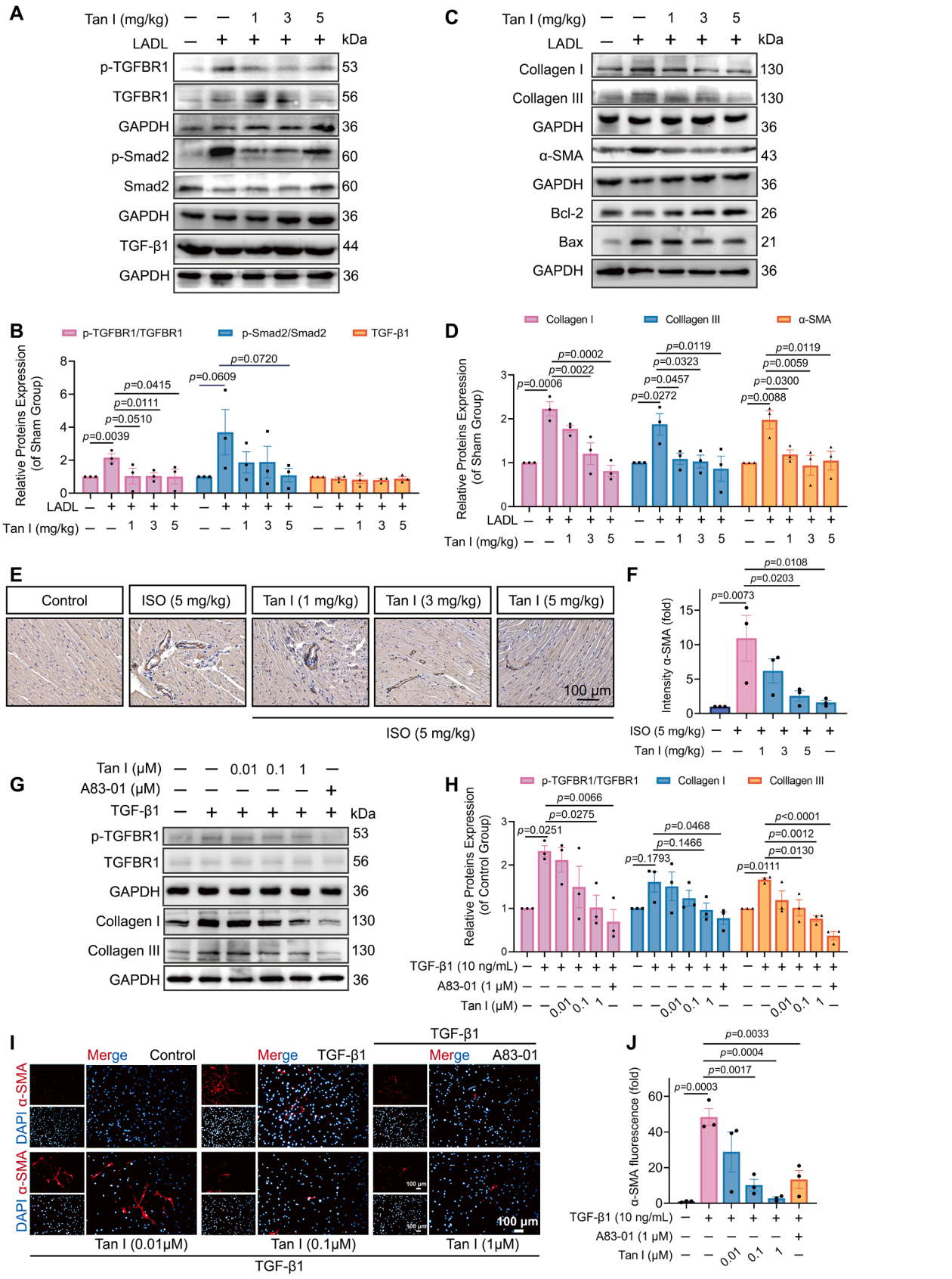

(caption on next page)

Fig. 5. Tan I inhibits the phosphorylation modification level of TGFBR1 and regulates the TGF-β signaling pathway and related proteins in cardiac tissues and NIH-3T3. (A, B) Representative WB images of TGFBR1, p-TGFBR1, Smad2, p-Smad2, and TGF-β1 in the hearts of each group of mice in the LADL model under Tan I (1, 3, and 5 mg/kg) intervention and quantitatively analyzed using image lab software ($n = 3$). (C, D) Representative WB images of Collagen I, Collagen III, α-SMA, Bax, and Bcl-2 in the hearts of each group of mice in the LADL model under Tan I (1, 3, and 5 mg/kg) intervention and quantitatively analyzed using image lab software ($n = 3$). (E, F) Representative images of α-SMA immunohistochemical staining in ISO model heart sections under Tan I (1, 3, and 5 mg/kg) intervention and quantification of α-SMA-positive areas (scale bar = 100 μm, $n = 3$). (G, H) Representative WB images of TGFBR1, p-TGFBR1, Collagen I, and Collagen III protein expression in NIH-3T3 cells treated with 10 ng/ml TGF-β1 for 24 h without or with Tan I (0.01, 0.1, and 1 μM) and 1 μM A83–01 and quantitatively analyzed using image lab software ($n = 3$). (I, J) Representative images of α-SMA IF staining without or with Tan I (0.01, 0.1, and 1 μM) and 1 μM A83–01 intervention in NIH-3T3 cells treated with 10 ng/ml TGF-β1 for 24 h and quantification of α-SMA-positive areas (scale bar = 100 μm, $n = 3$). Data are expressed as mean ± SEM.

pharmacology, Tan I may target TGFBR1 to regulate the related pathways of diabetes cardiomyopathy, especially the TGF-β signaling pathway, to perform its anti-MI role.

Tan I alleviates myocardial ischemia injury by modulating TGFBR1and TGF-β pathway signaling

The effects of Tan I on the TGFBR1/Smad classical pathway were further explored to determine the possible molecular mechanisms by which Tan I attenuated infarction in mice due to MI and MCF and improved cardiac function. The results reveal the elevated levels of phosphorylated TGFBR1 (p-TGFBR1) and phosphorylated Smad2 (p-Smad2) after myocardial infarction, whereas Tan I inhibited the phosphorylated modification of these proteins dose-dependently (Figs. 5A and 5B). Remarkably, the total expression of TGF - β1 and Smad2 proteins did not appear to change significantly. This implies that during MI and MCF, Tan I may only affect the activity of the target proteins rather than their total expression levels. (Figs. 5A, 5B, and S5A). Thus, the TGFBR1/Smad2 signaling pathway is activated after myocardial ischemic injury in mice, and Tan I can ameliorate LADL-induced MI and MCF by directly inhibiting the up-regulation of the level of the p-TGFBR1 protein, which results in the inhibition of the downstream signaling pathway.

The pathogenesis of MI and MCF involves multiple signaling pathways, in which apoptosis of cardiomyocytes and excessive synthesis and deposition of ECM are central processes. The experiments further verified the expressions of relevant proteins in the apoptotic pathway and collagen and α-SMA proteins. Compared with the Sham group mice, LADL induced MI mice showed a significant increase in the expression level of pro apoptotic protein Bax. Meanwhile, the anti-apoptotic protein Bcl-2 was down-regulated, and the expressions of α-SMA (F (4, 10) = 6.023, $p = 0.0119$), Collagen I (F (4, 10) = 15.58, $p = 0.0002$), and Collagen III (F (4, 10) = 4.501, $p = 0.0119$) were significantly up-regulated in the model group. However, Tan I-treated group dose-dependently reversed the expression levels of the above proteins towards the sham group (Figs. 5C, 5D and S5B). Similarly, ISO-induced MI and MCF in mice resulted in significantly higher expression level of α-SMA protein (F (4, 10) = 5.801, $p = 0.0073$), whereas the proportion of α-SMA-positive area was significantly reduced in the Tan I-treated group (F (4, 10) = 5.801, $p = 0.0108$) (Figs. 5E and 5F).

Collectively, these findings confirm the regulatory effects of Tan I on TGFBR1 and TGF-β signaling pathway and amelioration of the aberrant expressions of Bax, Bcl-2, Collagen I/III, and α-SMA proteins to attenuate MI injuries and MCF.

Tan I inhibits exogenous activation of TGFBR1 and related proteins to alleviate cardiomyocyte fibrosis

To explore the targeting effect of Tan I on TGFBR1 and its antifibrotic effect, we activated the TGFBR1 signaling pathway in NIH-3T3 fibroblasts by exogenous TGF-β1. Meanwhile, 1 μM A83–01, a selective TGFBR1 inhibitor (Chen et al., 2015; Huang et al., 2021), was used as a positive control. The results demonstrate that 10 ng/ml TGF-β1 exposure upregulated the phosphorylation level of TGFBR1 protein in NIH-3T3 (F (5, 12) = 5.364, $p = 0.0251$), whereas Tan I treatment decreased the expression level of p-TGFBR1 (F (5, 12) = 5.364, $p = 0.0066$) but did not change the total TGFBR1 protein expression (Figs. 5G and 5H). Notably, TGF-β1 induced Collagen I/III protein expressions in NIH-3T3 cells, which were remarkably higher than those in the control group, whereas Tan I dose-dependently decreased Collagen I (F (5, 12) = 2.662, $p = 0.0468$) and Collagen III (F (5, 12) = 11.75, $p < 0.0001$) protein expression (Figs. 5G and 5H, respectively). Additionally, the expression level of α-SMA protein was markedly enhanced in TGF-β1-stimulated NIH-3T3 cells (Figs. 5I and 5J), whereas Tan I significantly scaled down the positive area of α-SMA (F (5, 12) = 10.61, $p = 0.0004$). These results further suggest that Tan I can alleviate MCF. It achieves this by inhibiting the p-TGFBR1 protein, which in turn inhibits the expression of Collagen I, Collagen III and α-SMA.

Tan I inhibits cellular fibrosis caused by TGFBR1 OE in cells

OE of TGFBR1 in NIH-3T3 cells with LV-TGFBR1 was performed to further verify the targeting effect of Tan I inhibiting TGFBR1. The results revealed that after infection with LV-TGFBR1, significantly higher protein expression levels of TGFBR1 and p-TGFBR1 were observed relative to the negative control (NC) group. Nevertheless, the protein expression of p-TGFBR1 was down-regulated after treatment with 0.1 μM Tan I for 12 h (F (2, 2) = 4.318, $p = 0.0394$). The cells co-treated with A83–01 and Tan I showed a significant down-regulation of the p-TGFBR1 expression (F (2, 2) = 5.177, $p = 0.0396$) (Figs. 6A and 6B). Subsequently, the effects of Tan I on Smad2, α-SMA, Bcl-2, and Bax protein expression were further examined. Notably, Tan I ameliorated the abnormal level of protein expression caused by TGFBR1 OE (Figs. 6C–6F, S5C, and S5D). Meanwhile, the IF results show that the OE of TGFBR1 group enhanced the positive area of Collagen III, and the Tan I and A83–01 groups displayed significant reduction of fluorescence intensity (Figs. 6G and S5E).

To confirm that Tan I ameliorates cytofibrosis by inhibiting TGFBR1 and its relative signaling pathway, we further regulated TGFBR1 protein expression using exogenous TGF-β1 in the NIH-3T3 cells overexpressing TGFBR1. The results indicate that TGF-β1 stimulated a high TGFBR1 expression in the overexpressing TGFBR1 cells, whereas Tan I treatment partially inhibited the phosphorylation modification of TGFBR1 (Figs. 6H and 6I). The findings reveal that TGF-β1 stimulated high TGFBR1 expression in overexpressing TGFBR1 cells, and Tan I inhibited the phosphorylation modification of Smad2 protein (F(2, 2) = 1.523, $p = 0.0252$) (Figs. 6J and 6K), down-regulated the expression of α-SMA protein (Figs. S5F and S5G), ameliorated the aberrant expressions of Bcl-2 and Bax proteins (Figs. 6l and 6M), and reduced the positive area of Collagen III (Figs. 6N and S5H). Thus, these results further confirm that Tan I inhibits the expression of proteins, such as Collagen, α-SMA, and Smad2, by inactivating TGFBR1 and thereby inhibits TGF-β pathway signaling.

Tan I binds directly to TGFBR1

To further explore the properties of Tan I-TGFBR1 interaction, we analyzed the stability of the complex after Tan I–TGFBR1 interaction via molecular docking and MD simulations. The initial conformation for the simulations was set as the resultant complex in molecular docking of TGFBR1 with Tan I. Notably, the binding energy by molecular docking was -8.93 ± 0.02 kcal/mol with a pKi = 6.55, and the Tan I was stably bound in the cavity of TGFBR1 during the MD simulations at 0 and 50 ns

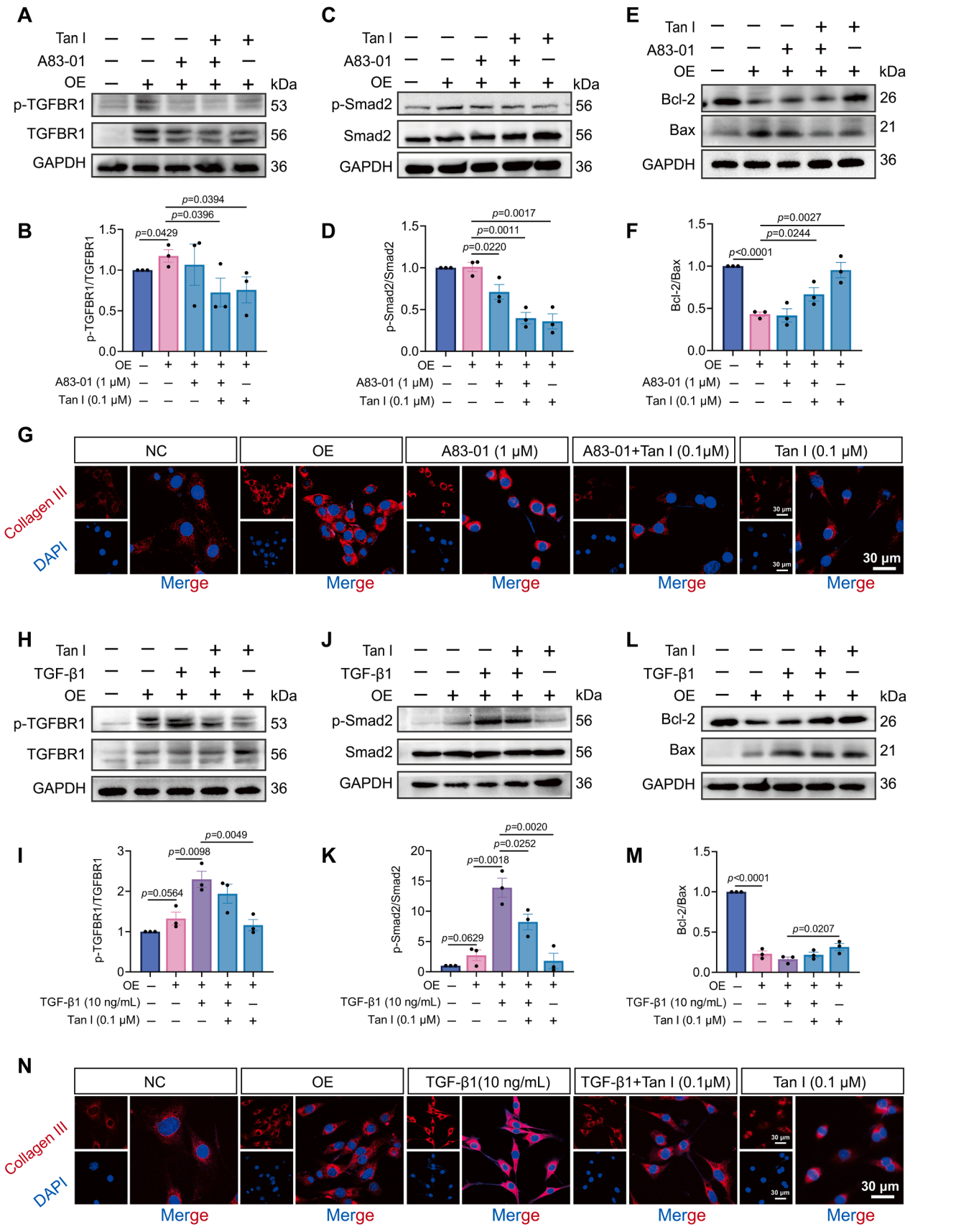

(caption on next page)

Fig. 6. Tan I and A83–01 or TGF-β1 intervene to regulate pathway signaling affected by TGFBR1 overexpression in NIH-3T3 cells. (A, B) Representative WB images of TGFBR1, p-TGFBR1 protein expression in NIH-3T3 cells overexpressing TGFBR1 without or with Tan I (0.1 μM) and A83–01 (1 μM), and quantitatively analyzed with Image lab software ($n = 3$). (C, D) Representative WB images of Smad2, p-Smad2 protein expression in NIH-3T3 cells overexpressing TGFBR1 without or with Tan I (0.1 μM) and A83–01 (1 μM), and quantitatively analyzed with Image lab software ($n = 3$). (E, F) Representative WB images of Bax and Bcl-2 protein expression in NIH-3T3 cells overexpressing TGFBR1 without or with Tan I (0.1 μM) an A83–01 (1 μM), and quantitatively analyzed with Image lab software ($n = 3$). (G) Representative images of Collagen III IF staining in Tan I or A83–01 interventions in NIH-3T3 (scale bar = 30 μm, $n = 3$). (H, I) Representative WB images of TGFBR1, p-TGFBR1 protein expression in NIH-3T3 cells overexpressing TGFBR1 without or with Tan I (0.1 μM) and TGF-β1 (10 ng/ml), and quantitatively analyzed with Image lab software ($n = 3$). (J, K) Representative WB images of Smad2, p-Smad2 protein expression in NIH-3T3 cells overexpressing TGFBR1 without or with Tan I (0.1 μM) and TGF-β1 (10 ng/ml), and quantitatively analyzed with Image lab software ($n = 3$). (L, M) Representative WB images of α-SMA, Bax, and Bcl-2 protein expression in NIH-3T3 cells overexpressing TGFBR1 without or with Tan I (0.1 μM) and TGF-β1 (10 ng/ml), and quantitatively analyzed with Image lab software ($n = 3$). (N) Representative images of Collagen III IF staining in Tan I or TGF-β1 interventions in NIH-3T3 (scale bar = 30 μm, $n = 3$). Data are expressed as mean ± SEM.

(Fig. 7A and Supplementary Video S1). The fluctuation of the RMSD (<0.2 nm) (Figs. 7B, and S6A) and RMSF (<0.3 nm) (Figs. 7C and S6B) values of the TGFBR1-Tan I and TGFBR1–A83–01 complexes tended to be stable, and the range was narrow, which implies an excellent stability. Gibbs energy landscape mapping analysis revealed that the TGFBR1–Tan I complex had a low-energy region, and the extent of this region is larger than that of the TGFBR1–A83–01 complex (Figs. 7D and 7E). Remarkably, the results of the BLI assay demonstrated that Tan I can bind to TGFBR1 in a dose-dependent manner, with a KD value of 1.5×10^{-6} M (Fig. 7F). Meanwhile, the results of CETSA show that after the binding of Tan I to the TGFBR1 protein, the stability of the complex was increased after 52 °C (Figs. 7G and 7H). Further, the findings indicate (Fig. 7I) that the luminescence (RLU) value of the reaction decreased rapidly with the increase in Tan I concentration, and the RLU value gradually stabilized after the reaction reached saturation (IC_{50}=739.6 nm) in the TGFBR1 kinase activity assay. Consistently, DARTS analysis indicated that Tan I-dependent gradient concentrations effectively reduced the sensitivity of TGFBR1 to the protease (Figs. 7J and 7K). These discoveries confirm that the binding between Tan I and TGFBR1 is robust and that Tan I can act directly on TGFBR1.

Discussion

MI is a major contributor to global cardiovascular deaths, and poses a major challenge to global public health (Travers et al., 2016). This condition is mainly caused by coronary artery occlusion and reduced myocardial blood flow, leading to disproportionate myocardial oxygen delivery and demand, which leads to myocardial cell reduction, necrosis, apoptosis, MCF, compensatory cardiac hypertrophy, and myocardial scarring (Zhang et al., 2023). Novel small-molecule drugs that prevent, attenuate, or reverse pathological myocardial fibrotic remodeling may provide directed clinical intervention for this CVD. *S. miltiorrhiza* is an extensively used Chinese herbal medicine. The results of numerous clinical and basic research have demonstrated that *S. miltiorrhiza* can prevent or treat ischemic CVDs, such as angina pectoris, myocardial infarction, and stroke, by inhibiting thrombosis, dilating coronary arteries, and increasing coronary artery blood flow (Orgah et al., 2020). Tan I represents one of the essential ingredients of *S. miltiorrhiza* with various pharmacological activities (Ke et al., 2023), including its capability to prevent and control CVD by improving the balance of the oxidant–antioxidant system (Wu et al., 2021), inhibiting vascular endothelial hyperplasia (Du et al., 2005), and suppressing the multiplication of vascular smooth muscle cells (Wang et al., 2005). Nevertheless, the pharmacodynamic effects and mechanisms of Tan I against MI have not been systematically described, and the exact mechanism of Tan I's action on MCF after MI is unclear.

To explore the cardioprotective effects of Tan I in heart, for the current study, we used LADL to construct the acute MI mouse model and induced chronic MI and fibrosis via the ISO subcutaneous injection method. Based on literature reports, the effective dose ranges for cardiovascular protection of Tan I and CAP are 1–10 (Jiang et al., 2022; Kim et al., 2009) and 10–20 mg/kg (Fang et al., 2024; Lu et al., 2023; Martino et al., 2011), respectively. Accordingly, we set up 1 (low dose), 3 (medium dose), 5 mg/kg Tan I (high dose) and a positive control CAP at 15 mg/kg in our animal experiments. We observed that Tan I improved functionality of the cardiac system in mice after acute and chronic MI, as evidenced by a reduction in ST-segment elevation and a modest recovery of the QRS waveform. In addition, Tan I alleviated the increase in cardiac heavy load, reduced the size of myocardial infarction, improved the degree of MCF, and regulated the level of myocardial injury markers, etc. In addition, the efficacy was better than that of the positive control group, which implies the unexplored potent *in vivo* efficacy of Tan I. We also conducted *in vitro* studies to further confirm that Tan I can effectively alleviate t-BHP-induced cellular oxidative stress due to its favorable antioxidant and anti-apoptotic effects.

To investigate the potential mechanism of the cardioprotective effect of Tan I, we integrated target fishing, molecular docking, bioinformatic analysis, and TMT-based proteomic approaches. Remarkably, we revealed the possible action of Tan I through the Smad-dependent classical TGF-β signaling pathway in diabetic cardiomyopathy signaling pathway, with TGFBR1 as a probable target of Tan I action. Specifically, TGF-β signaling is critical in several aspects of cardiac development, including inflammatory responses in cardiomyocytes, apoptosis, cardiac hypertrophy, fibrosis, and differentiation of cardiac progenitor cells, in which TGFBR1 performs a crucial function (Heger et al., 2016). Concisely, TGF-β ligands activate TGFBR2 phosphorylation and further promote the phosphorylation response of TGFBR1; such a condition triggers the phosphorylation and activation of Smad transcription factors, which further regulates multiple stages of cardiac development (Heger et al., 2016). Blockade of TGFBR1 activity attenuated cardiomyocyte apoptosis defects in mutant hearts *in vitro* (Peng et al., 2014). Yet, TGFBR1 can functionally regulate left ventricular remodeling (Boileau et al., 2018). Hence, in this study, the cardioprotective effect mechanism of Tan I in myocardial infarction mice was investigated through WB and IHC techniques. Tan I significantly reduced the level of p-TGFBR1 and its downstream signaling molecule p-Smad2 in mice after MI. Nevertheless, when the heart is subjected to pathological stress, cardiac fibroblasts can be transformed into activated myofibroblasts, which express α-SMA and synthesize ECM. The ECM is a complex network of structural proteins, such as Collagen I and III, elastin, and nonstructural proteins, such as fibronectin and laminin (Liu et al., 2024). Tan I also further modulated the aberrant expression levels of α-SMA, Collagen I, Collagen III, Bax, and Bcl-2 in the cardiac tissues of myocardial infarct mice to attenuate mouse MCF. To further investigate how Tan I affects the exogenous TGF-β1-induced fibrosis model in NIH-3T3 cells, we identified 10 ng/ml TGF-β1 (Chen et al., 2022) as an inducer and the positive control A83–01 (1 μM) as an inhibitor of TGFBR1 (Yamamura et al., 2012). Moreover, via WB and IF techniques, we observed that Tan I effectively inhibited the elevated phosphorylation of TGFBR1 caused by TGF-β1 stimulation and downregulated the expression levels of α-SMA, Collagen I, and Collagen III. Consistently, Tan I inhibited the up-regulation of TGFBR1 phosphorylation caused by OE of TGFBR1, attenuated downstream Smad2 signaling processes, and reduced collagen synthesis. Interestingly, the Tan I-only-treated group was superior to the A83–01-only-treated group. On the other hand, the Tan I and A83–01 co-treated groups inhibited signaling slightly better than the A83–01-only or Tan I-only-treated groups, and this finding may be attributed to the differences in the active sites of the two groups

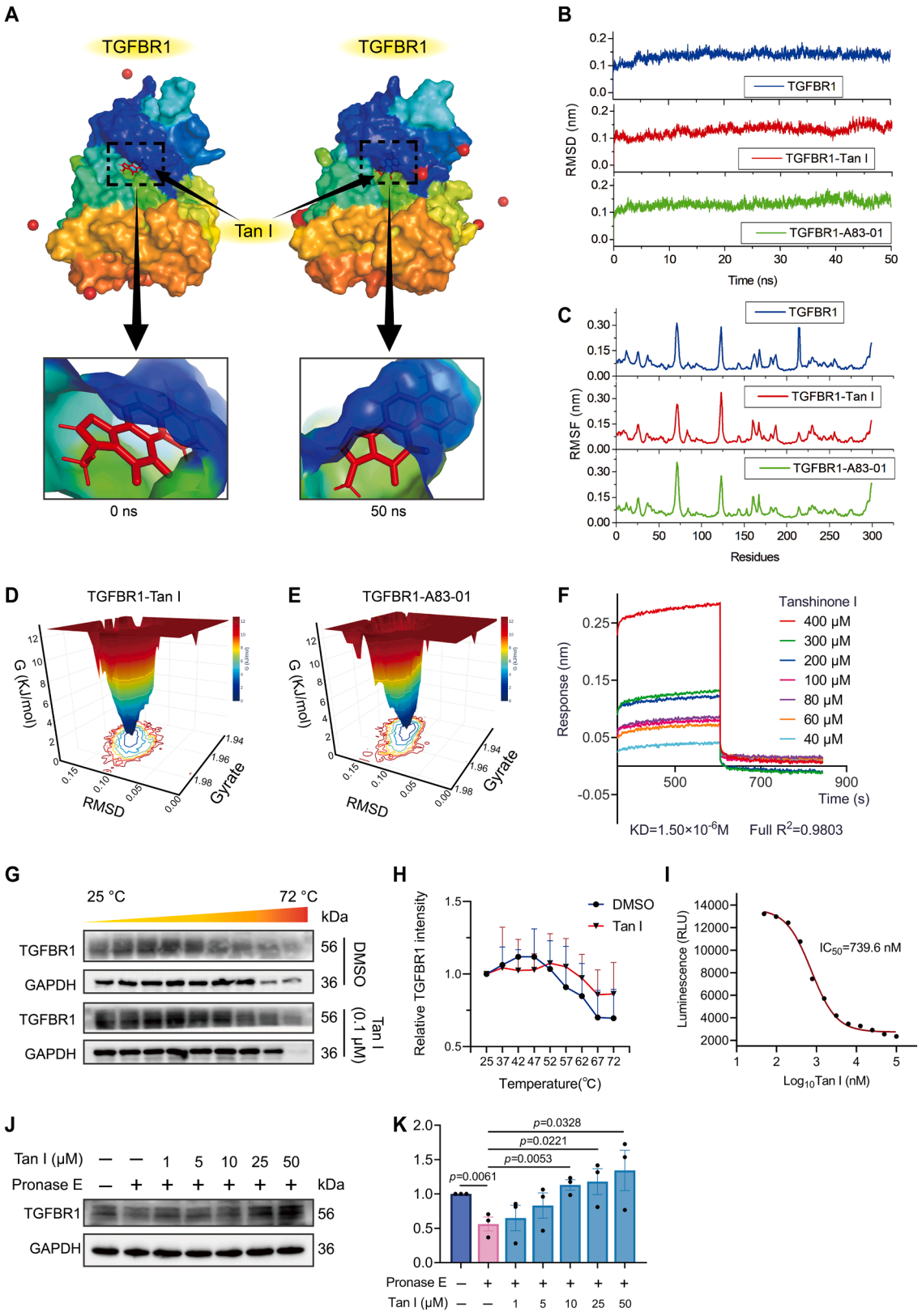

Fig. 7. Tan I interacts with TGFBR1 protein. (A) Binding conformation and interaction diagram between Tan I-TGFBR1 complexes at 0 and 50 ns. (B) RMSD of all atoms of TGFBR1 (blue) in complex with Tan I (red) or A83–01 (green). (C) RMSF of all atoms of TGFBR1 (blue) in complex with Tan I (red) or A83–01 (green). (D) Gibbs energy landscape 3D mapping of TGFBR1 protein with Tan I. (E) Gibbs energy landscape 3D mapping of TGFBR1 protein with Tan I. (F) Sensorgram for BLI testing of TGBFR1 specific binding to Tan I. (G, H) Representative WB images of Tan I (0.1 μM) and TGFBR1 from the CETSA (NIH-3T3 cells, at 25 to 72 °C) and quantitatively analyzed using Image lab software ($n = 3$). (I) Inhibitory effect of Tan I on TGFBR1 kinase activity. (J, K) Effect of Tan I on TGFBR1 in Pronase E-treated H9c2 cells. Data are expressed as mean ± SEM.

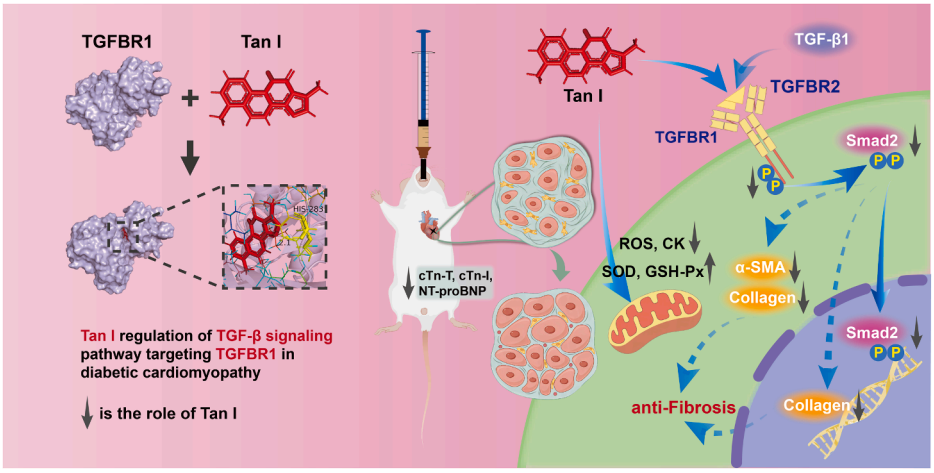

Fig. 8. Tanshinone I alleviates post-ischemic myocardial injury by targeting TGFBR1 and modulating the TGF-β signaling pathway.

acting on the TGFBR1 protein, which produced an excellent combined inhibitory effect. Similarly, Tan I inhibited to a certain degree the TGF-β1-induced TGFBR1 phosphorylation modification and downstream signaling processes in TGFBR1-overexpressing NIH-3T3 cells. Finally, we confirmed the multidimensional interaction between Tan I and TGFBR1 via MD simulation, BLI technique, CETSA, enzyme inhibition, and DARTS assays, *i.e.*, Tan I is probably a potential inhibitor of TGFBR1. Therefore, for the first time, our study revealed in detail the mechanism of action of Tan I on MCF after MI. Briefly, Tan I prevents and treats undesirable cardiac remodeling and collagen deposition following MI by inhibiting the Smad-dependent canonical TGF-β signaling pathway, of which TGFBR1 is a potential target protein, thereby affecting downstream signaling. Our findings not only provide a new theoretical basis for Tan I as a potential cardioprotective drug but also offer new targets and research directions for future MI and MCF therapeutic strategies. Fig. 8 presents the proposed and validated mechanism of action of Tan I in exerting its anti-MI and anti-MCF effects.

However, there are certain limitations to this study. The current work is based on a mouse model, and the feasibility of translating the results to human clinical applications needs to be further investigated. Although our current research explored the key target pathways of Tan I in MI, it did not comprehensively analyze the complex pathogenesis of the disease. Certainly, pharmacokinetic characterization with Tan I is essential before the optimization of dosing regimens in future clinical trials. These limitations need to be addressed in future studies to ensure the efficacy and safety of Tan I in the treatment of myocardial ischemic disease.

Conclusion

The present study validated the favorable therapeutic effects of Tan I against MI through *in vivo* dual-model and *in vitro* dual-cell experiments. Importantly, the present work utilized network pharmacology and TMT-based proteomics techniques to predict TGFBR1 as the possible target of Tan I action. Furthermore, mechanistic validation confirmed that Tan I can regulate Smad2 and other proteins related to TGF-β pathway signaling by inhibiting the level of phosphorylation modification of TGFBR1 in cardiac tissues of MI mice. Notably, the molecular interaction results observed in MD simulation, BLI technique, CETSA, enzyme inhibition, and DARTS assays further corroborate the stability of Tan I binding to TGFBR1. These findings indicate that Tan I may act on TGFBR1 and affect the signaling pathway, which may ultimately alleviate myocardial infarction and fibrosis caused by MI and improve ventricular remodeling. It can also contribute to an improved understanding of the mechanism and value of Tan I in the treatment of CVDs and provide the foundation for the clinical application and exploitation of Tan I and traditional Chinese medicinal preparations containing *S. miltiorrhiza*.

Author statement

All data were generated in-house, and no paper mill was used. All authors agree to be accountable for all aspects of work ensuring integrity and accuracy.

CRediT authorship contribution statement

Liyuan Ke: Writing – original draft, Visualization, Methodology, Investigation, Formal analysis. **Ziyao Zheng:** Validation, Investigation. **Shumin Ye:** Validation, Investigation. **Chenhui Zhong:** Validation. **Qingyun Lin:** Validation. **Yan Hu:** Resources. **Peiying Shi:** Writing – review & editing, Funding acquisition, Data curation. **Lei Wen:** Writing – review & editing, Funding acquisition. **Hong Yao:** Writing – review & editing, Supervision, Resources, Project administration, Funding acquisition, Formal analysis, Data curation, Conceptualization.

Declaration of competing interest

The authors declare that they have no known competing financial interests or personal relationships that could have appeared to influence the work reported in this paper.

Acknowledgements

This work was supported by National Natural Science Foundation of China (Grants No: 81973558 and 82205078), and Natural Science Foundation of Fujian province (2023J01075). We sincerely appreciate the technical support provided by the Public Technology Service Center, Fujian Medical University and researcher Hou Ping from the Institute of Immunotherapy.

Supplementary materials

Supplementary material associated with this article can be found, in the online version, at doi:10.1016/j.phymed.2025.156994.

References

Anzai, A., Choi, J.L., He, S., Fenn, A.M., Nairz, M., Rattik, S., McAlpine, C.S., Mindur, J. E., Chan, C.T., Iwamoto, Y., Tricot, B., Wojtkiewicz, G.R., Weissleder, R., Libby, P., Nahrendorf, M., Stone, J.R., Becher, B., Swirski, F.K., 2017. The infarcted myocardium solicits GM-CSF for the detrimental oversupply of inflammatory leukocytes. J. Exp. Med. 214, 3293–3310. https://doi.org/10.1084/jem.20170689.

Bai, H., Lyu, J., Nie, X., Kuang, H., Liang, L., Jia, H., Zhou, S., Li, C., Li, T., 2023. Ginsenoside Rg5 enhances the radiosensitivity of lung adenocarcinoma via reducing HSP90-CDC37 interaction and promoting client protein degradation. J. Pharm. Anal. 13, 1296–1308. https://doi.org/10.1016/j.jpha.2023.06.004.

Boileau, A., Lalem, T., Vausort, M., Zhang, L., Devaux, Y., 2018. A 3-gene panel improves the prediction of left ventricular dysfunction after acute myocardial infarction. Int. J. Cardiol. 254, 28–35. https://doi.org/10.1016/j.ijcard.2017.10.109.

Chen, G., Xu, H., Xu, T., Ding, W., Zhang, G., Hua, Y., Wu, Y., Han, X., Xie, L., Liu, B., Zhou, Y., 2022. Calycosin reduces myocardial fibrosis and improves cardiac function in post-myocardial infarction mice by suppressing TGFBR1 signaling pathways. Phytomedicine 104, 154277. https://doi.org/10.1016/j.phymed.2022.154277.

Chen, X., Yu, J., Zhong, B., Lu, J., Lu, J.-J., Li, S., Lu, Y., 2019. Pharmacological activities of dihydrotanshinone I, a natural product from *Salvia miltiorrhiza* Bunge. Pharmacol. Res. 145, 104254. https://doi.org/10.1016/j.phrs.2019.104254.

Deng, B., Wang, K., He, H., Xu, M., Li, J., He, P., Liu, Y., Ma, J., Zhang, J., Dong, W., 2025. Biochanin A mitigates colitis by inhibiting ferroptosis-mediated intestinal barrier dysfunction, oxidative stress, and inflammation via the JAK2/STAT3 signaling pathway. Phytomedicine 156699. https://doi.org/10.1016/j.phymed.2025.156699.

Du, J., Li, X., Zhang, R., Qian, Z., 2005. Tanshinone inhibits intimal hyperplasia in the ligated carotid artery in mice. J. Ethnopharmacol. 98, 319–322. https://doi.org/10.1016/j.jep.2005.01.038.

Edsfeldt, A., Singh, P., Matthes, F., Tengryd, C., Cavalera, M., Bengtsson, E., Dunér, P., Volkov, P., Karadimou, G., Gisterå, A., Orho-Melander, M., Nilsson, J., Sun, J., Gonçalves, I., 2023. Transforming growth factor-β2 is associated with atherosclerotic plaque stability and lower risk for cardiovascular events. Cardiovasc. Res. 119, 2061–2073. https://doi.org/10.1093/cvr/cvad079.

Eladwy, R.A., Mantawy, E.M., El-Bakly, W.M., Fares, M., Ramadan, L.A., Azab, S.S., 2018. Mechanistic insights to the cardioprotective effect of blueberry nutraceutical extract in isoprenaline-induced cardiac hypertrophy. Phytomedicine 51, 84–93. https://doi.org/10.1016/j.phymed.2018.10.009.

Fang, R., Zhou, R., Ju, D., Li, M., Wang, H., Pan, L., Wang, X., Han, M., Yu, Y., 2024. Zhen-wu-tang protects against myocardial fibrosis by inhibiting M1 macrophage polarization via the TLR4/NF-κb pathway. Phytomedicine 130, 155719. https://doi.org/10.1016/j.phymed.2024.155719.

Francis, R., Kalyanaraman, R., Boominathan, V., Parthasarathy, S., Chavaan, A., Ansari, I.A., Ansari, S.A., Alkahtani, H.M., Chandran, J., Tharumasivam, S.V., 2024. Piperine's potential in treating polycystic ovarian syndrome explored through in-silico docking. Sci. Rep. 14, 21834. https://doi.org/10.1038/s41598-024-72800-6.

Gao, C., Xu, Y., Liang, Z., Wang, Y., Shang, Q., Zhang, S., Wang, C., Ni, M., Wu, D., Huang, Z., Pang, T., 2021. A novel PGAM5 inhibitor LFHP-1c protects blood–brain barrier integrity in ischemic stroke. Acta Pharm. Sin. B 11, 1867–1884. https://doi.org/10.1016/j.apsb.2021.01.008.

Gao, E., Lei, Y.H., Shang, X., Huang, Z.M., Zuo, L., Boucher, M., Fan, Q., Chuprun, J.K., Ma, X.L., Koch, W.J., 2010. A novel and efficient model of coronary artery ligation and myocardial infarction in the mouse. Circ. Res. 107, 1445–1453. https://doi.org/10.1161/CIRCRESAHA.110.223925.

Han, D., Wang, F., Shen, D., 2024. Nanomedicines as guardians of the heart: unleashing the power of antioxidants to alleviate myocardial ischemic injury. Theranostics 14, 5336–5370. https://doi.org/10.7150/thno.99961.

Heger, J., Schulz, R., Euler, G., 2016. Molecular switches under tgfβ signalling during progression from cardiac hypertrophy to heart failure. Brit. J Pharmacol. 173, 3–14. https://doi.org/10.1111/bph.13344.

Jiang, Q., Chen, X., Tian, X., Zhang, J., Xue, S., Jiang, Y., Liu, T., Wang, X., Sun, Q., Hong, Y., Li, C., Guo, D., Wang, Y., Wang, Q., 2022. Tanshinone I inhibits doxorubicin-induced cardiotoxicity by regulating Nrf2 signaling pathway. Phytomedicine 106, 154439. https://doi.org/10.1016/j.phymed.2022.154439.

Kalyanaraman, R., Boominathan, V., Francis, R., Parthasarathy, S., Chandran, J., Tharumasivam, S.V., 2024. *In vivo* molecular functional aging and gradual senescence with hTERT gene as antiaging interventions in Danio rerio. UPJOZ 45, 371–389. https://doi.org/10.56557/upjoz/2024/v45i184456.

Ke, L., Zhong, C., Chen, Z., Zheng, Z., Li, S., Chen, B., Wu, Q., Yao, H., 2023. Tanshinone I: pharmacological activities, molecular mechanisms against diseases and future perspectives. Phytomedicine 110, 154632. https://doi.org/10.1016/j.phymed.2022.154632.

Kim, D.H., Kim, S., Jeon, S.J., Son, K.H., Lee, S., Yoon, B.H., Cheong, J.H., Ko, K.H., Ryu, J.H., 2009. Tanshinone I enhances learning and memory, and ameliorates memory impairment in mice via the extracellular signal-regulated kinase signalling pathway. Brit. J Pharmacol. 158, 1131–1142. https://doi.org/10.1111/j.1476-5381.2009.00378.x.

Krishnasamy, G., Parthasarathy, S., Rajasekaran, S., Raja, T.W., Andrea, S.G., Tharumasivam, S.V., 2024. Evaluation of potential EGFR inhibitors for non-small cell lung cancer: a structure-based virtual screening and molecular dynamics study. J. Pharm. Res. Int. 36, 253–263. https://doi.org/10.9734/jpri/2024/v36i117617.

Lee, T.-L., Lai, T.-C., Lin, S.-R., Lin, S.-W., Chen, Y.-C., Pu, C.-M., Lee, I.-T., Tsai, J.-S., Lee, C.-W., Chen, Y.-L., 2021. Conditioned medium from adipose-derived stem cells attenuates ischemia/reperfusion-induced cardiac injury through the microRNA-221/222/PUMA/ETS-1 pathway. Theranostics 11, 3131–3149. https://doi.org/10.7150/thno.52677.

Li, S., Liu, H., Lin, Z., Li, Z., Chen, Y., Chen, B., Huang, L., Lin, X., Yao, H., 2022. Isoorientin attenuates doxorubicin-induced cardiac injury via the activation of MAPK, Akt, and Caspase-dependent signaling pathways. Phytomedicine 101, 154105. https://doi.org/10.1016/j.phymed.2022.154105.

Liu, Z., Bian, X., Li, L., Liu, L., Feng, C., Wang, Ying, Ni, J., Li, S., Lu, D., Li, Y., Ma, C., Yu, T., Xiao, X., Xue, N., Wang, Yuxiang, Zhang, C., Ma, X., Gao, X., Fan, X., Liu, X., Fan, G., 2024. SENP1-Mediated HSP90ab1 DeSUMOylation in cardiomyocytes prevents myocardial fibrosis by paracrine signaling. Adv. Sci., 2400741 https://doi.org/10.1002/advs.202400741.

Lu, H., Jiang, X., He, L., Ji, X., Li, X., Liu, S., Sun, Y., Qin, X., Xiong, X., Philipsen, S., Xi, B., Zhang, M., Yang, J., Zhang, C., Zhang, Y., Zhang, W., 2023. Endothelial Sp1/Sp3 are essential to the effect of captopril on blood pressure in male mice. Nat. Commun. 14, 5891. https://doi.org/10.1038/s41467-023-41567-1.

Martino, T.A., Tata, N., Simpson, J.A., Vanderlaan, R., Dawood, F., Kabir, M.G., Khaper, N., Cifelli, C., Podobed, P., Liu, P.P., Husain, M., Heximer, S., Backx, P.H., Sole, M.J., 2011. The primary benefits of angiotensin-converting enzyme inhibition on cardiac remodeling occur during sleep time in murine pressure overload hypertrophy. J. Am. Coll. Cardiol. 57, 2020–2028. https://doi.org/10.1016/j.jacc.2010.11.022.

Orgah, J.O., He, S., Wang, Yule, Jiang, M., Wang, Yuefei, Orgah, E.A., Duan, Y., Zhao, B., Zhang, B., Han, J., Zhu, Y., 2020. Pharmacological potential of the combination of *Salvia miltiorrhiza* (Danshen) and Carthamus tinctorius (Honghua) for diabetes mellitus and its cardiovascular complications. Pharmacol. Res. 153, 104654. https://doi.org/10.1016/j.phrs.2020.104654.

Peng, Y., Song, L., Zhao, M., Harmelink, C., Debenedittis, P., Cui, X., Wang, Q., Jiao, K., 2014. Critical roles of miRNA-mediated regulation of TGF signalling during mouse cardiogenesis. Cardiovasc. Res. 103, 258–267. https://doi.org/10.1093/cvr/cvu126.

Qu, C., Xu, Q.-Q., Yang, W., Zhong, M., Yuan, Q., Xian, Y.-F., Lin, Z.-X., 2023. Gut dysbiosis aggravates cognitive deficits, amyloid pathology and lipid metabolism dysregulation in a transgenic mouse model of Alzheimer's disease. J. Pharm. Anal. 13, 1526–1547. https://doi.org/10.1016/j.jpha.2023.07.014.

Travers, J.G., Kamal, F.A., Robbins, J., Yutzey, K.E., Blaxall, B.C., 2016. Cardiac fibrosis: the fibroblast awakens. Circ. Res. 118, 1021–1040. https://doi.org/10.1161/CIRCRESAHA.115.306565.

Travers, J.G., Tharp, C.A., Rubino, M., McKinsey, T.A., 2022. Therapeutic targets for cardiac fibrosis: from old school to next-gen. J. Clin. Investigat. 132, e148554. https://doi.org/10.1172/JCI148554.

Velmurugan, G., Dinakaran, V., Rajendhran, J., Swaminathan, K., 2020. Blood microbiota and circulating microbial metabolites in diabetes and cardiovascular disease. Trend. Endocrinol. Metabol. 31, 835–847. https://doi.org/10.1016/j.tem.2020.01.013.

Wang, H., Gao, X., Zhang, B., 2005. Tanshinone: an inhibitor of proliferation of vascular smooth muscle cells. J. Ethnopharmacol. 99, 93–98. https://doi.org/10.1016/j.jep.2005.01.057.

Wu, Y., Bi, Y.-M., Tan, Z.-B., Xie, L.-P., Xu, H.-L., Fan, H.-J., Chen, H.-M., Li, J., Liu, B., Zhou, Y.-C., 2019. Tanshinone I inhibits vascular smooth muscle cell proliferation by targeting insulin-like growth factor-1 receptor/phosphatidylinositol-3-kinase signaling pathway. Eur. J. Pharmacol. 853, 93–102. https://doi.org/10.1016/j.ejphar.2019.03.021.

Wu, Y.-T., Xie, L.-P., Hua, Y., Xu, H.-L., Chen, G.-H., Han, X., Tan, Z.-B., Fan, H.-J., Chen, H.-M., Li, J., Liu, B., Zhou, Y.-C., 2021. Tanshinone I inhibits oxidative stress–Induced cardiomyocyte injury by modulating Nrf2 signaling. Front. Pharmacol. 12, 644116. https://doi.org/10.3389/fphar.2021.644116.

Xiang, X., Cai, H.-D., Su, S., Dai, X., Zhu, Y., Guo, J., Yan, H., Guo, S., Gu, W., Qian, D., Tang, Z., Duan, J., 2019. Salvia miltiorrhiza protects against diabetic nephropathy through metabolome regulation and wnt/β-catenin and TGF-β signaling inhibition. Pharmacol. Res. 139, 26–40. https://doi.org/10.1016/j.phrs.2018.10.030.

Xie, R., Li, C., Zhong, C., Lin, Z., Li, S., Chen, B., Wu, Y., Hu, F., Shi, P., Yao, H., 2024. Integration of virtual screening and proteomics reveals potential targets and pathways for ginsenoside Rg1 against myocardial ischemia. J. Ginseng. Res. 48, 395–404. https://doi.org/10.1016/j.jgr.2024.02.001.

Yamamura, S., Matsumura, N., Mandai, M., Huang, Z., Oura, T., Baba, T., Hamanishi, J., Yamaguchi, K., Kang, H.S., Okamoto, T., Abiko, K., Mori, S., Murphy, S.K., Konishi, I., 2012. The activated transforming growth factor-beta signaling pathway in peritoneal metastases is a potential therapeutic target in ovarian cancer. Intl. J. Cancer 130, 20–28. https://doi.org/10.1002/ijc.25961.

Yang, A., Zeng, K., Huang, H., Liu, Dongxiao, Song, X., Qian, Y., Yu, X., Liu, Dan, Zha, X., Zhang, H., Chai, X., Tu, P., Hu, Z., 2023. Usenamine A induces apoptosis and autophagic cell death of human hepatoma cells via interference with the Myosin-9/actin-dependent cytoskeleton remodeling. Phytomedicine 116, 154895. https://doi.org/10.1016/j.phymed.2023.154895.

Zhang, L., Li, T., Yu, Y., Shi, K., Bei, Z., Qian, Y., Qian, Z., 2023. An injectable conductive hydrogel restores electrical transmission at myocardial infarct site to preserve cardiac function and enhance repair. Bioact. Mater. 20, 339–354. https://doi.org/10.1016/j.bioactmat.2022.06.001.

Zhao, W., Feng, H., Sun, W., Liu, K., Lu, J.-J., Chen, X., 2017. Tert-butyl hydroperoxide (t-BHP) induced apoptosis and necroptosis in endothelial cells: roles of NOX4 and mitochondrion. Redox Biol. 11, 524–534. https://doi.org/10.1016/j.redox.2016.12.036.

Zhong, C., Ke, L., Hu, F., Lin, Zuan, Ye, S., Zheng, Z., Han, S., Lin, Zan, Zhan, Y., Hu, Y., Shi, P., Wen, L., Yao, H., 2025. Ginsenoside Rb1 inhibits cardiomyocyte apoptosis and rescues ischemic myocardium by targeting caspase-3. J. Pharm. Anal. 15, 101142. https://doi.org/10.1016/j.jpha.2024.101142.

Zhou, Y., Dai, Z., Deng, K., Wang, Y., Ying, J., Chu, D., Zhou, J., Tang, C., 2023. Eight Zhes Decoction ameliorates the lipid dysfunction of nonalcoholic fatty liver disease using integrated lipidomics, network pharmacology and pharmacokinetics. J. Pharm. Anal. 13, 1058–1069. https://doi.org/10.1016/j.jpha.2023.05.012.

Zhu, C., Cai, T., Jin, Y., Chen, J., Liu, G., Xu, N., Shen, R., Chen, Y., Han, L., Wang, S., Wu, C., Zhu, M., 2020. Artificial intelligence and network pharmacology based investigation of pharmacological mechanism and substance basis of Xiaokewan in treating diabetes. Pharmacol. Res. 159, 104935. https://doi.org/10.1016/j.phrs.2020.104935.